# Functional architecture of the pancreatic islets reveals first responder cells which drive the first-phase [$Ca^{2+}$] response

**Vira Kravets[a,b,1], JaeAnn M. Dwulet[a], Wolfgang E. Schleicher[b], David J. Hodson[c], Anna M. Davis[a], Laura Pyle[d], Robert A. Piscopio[b], Maura Sticco-Ivins,[b] Richard K.P. Benninger[a,b,1].**

[a] Department of Bioengineering, University of Colorado, Anschutz Medical Campus, Aurora, CO. USA

[b] Barbara Davis center for childhood diabetes, University of Colorado, Anschutz Medical campus, Aurora, CO. USA

[c] Institute of Metabolism and Systems Research, University of Birmingham, Birmingham. UK, and Centre for Endocrinology, Diabetes and Metabolism, Birmingham Health Partners, Birmingham, UK

[d] Department of Pediatrics, University of Colorado School of Medicine, Department of Biostatistics and Informatics, Colorado School of Public Health

[1] To whom correspondence should be addressed:
richard.benninger@cuanschutz.edu and vira.kravets@cuanschutz.edu
Tel: (303) 724-6388. Fax: (303) 724-5800.
1775 Aurora court, University of Colorado Anschutz Medical campus, Aurora, CO. 80045.

**Short title:** First responder cells control islet function

**Keywords:** Laser ablation; Multicellular Dynamics; Biological Networks; Optical Microscopy; Diabetes; Gap junctions.

**Abstract**

Insulin-secreting β-cells are functionally heterogeneous. Whether there exist cells driving the first-phase calcium response in individual islets, has not been examined. We examine 'first responder' cells, defined by the earliest [$Ca^{2+}$] response during first-phase [$Ca^{2+}$] elevation, distinct from previously identified "hub" and "leader" cells. First responder cells showed characteristics of high membrane excitability and lower electrical coupling to their neighbors. The first-phase response time of β-cells in the islet was spatially organized, dependent on the cell's distance to the first responder cell, and consistent over time up to ~24 h. When first responder cells were laser ablated, the first-phase [$Ca^{2+}$] was slowed down, diminished, and discoordinated compared to random cell ablation. Cells that were next earliest to respond often took over the role of the first responder upon ablation. In summary, we discover and characterize a distinct first responder β-cell state, critical for the islet first-phase response to glucose.

## Introduction:

Diabetes Mellitus is a disease characterized by high blood glucose, caused by insufficient secretion of insulin. β-cells within pancreatic islets of Langerhans secrete insulin and are compromised in diabetes. Early work showed that in mechanically-dispersed islets, single β-cells are heterogeneous in the level of insulin release [1]. More recent studies have discovered markers that separate β-cells into distinct populations with differing functional properties. This includes markers that subdivides proliferative-competent β-cells from mature β-cells [2]; subdivides β-cells with different levels of insulin gene expression, granularity and secretion [3]; or subdivides β-cells that have differing responsiveness to insulin secretagogues [4]. Furthermore, single-cell high-throughput approaches such as single cell RNA sequencing (scRNAseq) or mass cytometry separate distinct β-cell populations [5, 6]. However, the role of the heterogeneity in the function of the islet is poorly understood.

β-cells are excitable and show elevated electrical activity in response to glucose. Following metabolism of glucose, ATP-sensitive potassium channels ($K_{ATP}$) close, depolarizing the membrane. This membrane depolarization opens voltage-gated calcium channels, elevating intra-cellular free $Ca^{2+}$ activity ($[Ca^{2+}]$) and triggering insulin release. β-cells are electrically coupled to neighboring β-cells via Connexin36 (Cx36) gap junction channels [7-11], which enables the direct exchange of cations between β-cells [12]. Under low glucose conditions, gap junction channels transmit hyperpolarizing currents that suppress islet electrical activity and insulin release [13-15]. Under elevated glucose gap junction channels coordinate the oscillatory dynamics of islet electrical activity, thereby enhancing first-phase insulin and pulsatile second-phase insulin, and glucose tolerance [11, 16].

59 Gap junction coupling is non-uniform throughout the islet [17]. β-cells are also
60 heterogeneous in glucose metabolism and excitability [18]. As a result, at low glucose some β-
61 cells are suppressed more than others by hyperpolarizing currents transmitted from neighboring
62 cells [19]. Conversely at elevated glucose, some β-cells are recruited and/or coordinated more than
63 others by depolarizing currents transmitted from neighboring cells. As such, the response of each
64 β-cell within the islet to glucose is different, reflecting both its intrinsic heterogeneity and its
65 context within the islet. Several studies have sought to identify and characterize functional β-cell
66 states within the islet based on the [$Ca^{2+}$] response under glucose stimulation, together with the
67 use of optogenetic based constructs and laser ablation. For example, β-cells that show significantly
68 increased connectivity, termed 'hubs' or 'hub cells' [20, 21], disproportionately suppressed islet
69 [$Ca^{2+}$] following targeted hyper-polarization via optogenetic stimulation. Conversely a population
70 of β-cells disproportionately activated islet [$Ca^{2+}$] following targeted depolarization via
71 optogenetic stimulation [22]. Furthermore, cells that show [$Ca^{2+}$] oscillations that precede the rest
72 of the islet, termed 'leader' cells or 'wave-origin' [22-24], have also been suggested to drive the
73 oscillatory dynamics of [$Ca^{2+}$].

74 Both in rodents and in humans, first and second phases of insulin secretion have been
75 distinguished [25, 26]. Glucose-stimulated [$Ca^{2+}$] influx into the cell is necessary for both first and
76 second phases of insulin secretion [27]. β-cell [$Ca^{2+}$] is also bi-phasic [28] and is correlated with
77 insulin secretion dynamics [29]. The first-phase of [$Ca^{2+}$] response following low-to-high glucose
78 is *transitional*, where cells with intrinsic differences in metabolic activity or other properties may
79 be responding differently. The second-phase [$Ca^{2+}$] response at high glucose is *steady-state* where
80 the majority of cells are equally likely to fire [14], but with [$Ca^{2+}$] oscillations showing differing
81 amplitudes, temporal delay (phase lag), and oscillation frequency [30, 31]. While different β-cell

82 subpopulations have been examined during this second-phase [$Ca^{2+}$] response, the role of
83 functional β cell states during the first-phase [$Ca^{2+}$] has not been examined.

84 Here we identify functional β-cell state based on cell dynamics during the first-phase [$Ca^{2+}$]
85 response to glucose, and test whether they disproportionately affect islet function. We address
86 what mechanisms underlie their properties and disproportionate effect on islet function and ask
87 whether they overlap with other identified β-cell states.

88 **Results:**

89 *First responder cells are distinct from β-cell functional states associated with second-phase*
90 *[$Ca^{2+}$].* We first sought to identify β-cells that may exert control over the first-phase [$Ca^{2+}$]
91 response, and test whether they differ from cells reported to control the second-phase [$Ca^{2+}$]
92 response. [$Ca^{2+}$] dynamics were recorded using confocal microscopy in the two-dimensional islet
93 plane (Fig.1 A) continuously before and after glucose stimulation in islets isolated from Mip-
94 $Cre^{ER}$; Rosa-Stop-Lox-Stop-GCamP6s mice (β-GCamP6s) that show β-cell specific GCamP6s
95 expression following tamoxifen-induced CreER-mediated recombination. We quantified the
96 response time to glucose for each cell using initial [$Ca^{2+}$] elevation (Fig.1 B) and defined the '*first*
97 *responder*' cells as 10% of cells in the islet with fastest response to glucose elevation, $T_{resp}$ (Fig.1
98 C and methods). The '*last responder*' cells were defined as 10% of islet cells with latest response.
99 The $T_{resp}$ distribution varied between the islets. The fastest 25% percentile preceded the islet-
100 median response by ~10 seconds, whereas the slowest 25% percentile lagged the islet-median by
101 about the same amount of time (see cumulative $T_{resp}$ distribution for multiple islets in Fig.S1 A).
102 First responder cells were located closer to the islet periphery (Fig.S1 B). Islets from the β-
103 GCamP6s mice demonstrated a bi-phasic [$Ca^{2+}$] response to glucose elevation, with the first phase
104 characterized by a steep [$Ca^{2+}$] rise and subsequent plateau (Fig.1 D red rectangle), and the second,
105 oscillatory phase characterized by [$Ca^{2+}$] wave (Fig.1 D blue rectangle). Some islets didn't have a
106 robust [$Ca^{2+}$] wave (see methods).

107 We next examined the overlap between properties of cells defined by the first-phase and
108 second-phase [$Ca^{2+}$] dynamics. During the oscillatory second phase, highly connected "hub cells"
109 have been implicated in maintaining [$Ca^{2+}$] elevations. To assess whether first responder cells
110 overlap with these "hub" cells, we identified "hub-like (phase2)" cells via network analysis as

111 performed previously [20] (Fig.1 E). '*Leader*' cells, which have previously been defined and
112 characterized [22, 24], were defined as 10% of all cells with highest *negative* phase lag, which
113 corresponds to showing an earlier [$Ca^{2+}$] oscillation (Fig.S1 C, D).

114 The response times of leader and hub-like(ph2) cells were no different from the islet
115 average (Fig. 1F), *i.e.,* they did not lead the first-phase [$Ca^{2+}$] response to glucose. While the first
116 responder cells had significantly different $T_{resp}$ compared to the islet-average cell (p=0.0105).
117 During the second-phase [$Ca^{2+}$] dynamics, the *phase lag* of the [$Ca^{2+}$] wave of the hub-like(ph2)
118 cells was no different from the islet average (Fig1 G), *i.e.,* they did not lead the second-phase
119 [$Ca^{2+}$] response to glucose. Interestingly, the first responder and leader cells had phase lag which
120 was substantially different from that of islet-average (p=0.0476 and p<0.0001 correspondingly),
121 indicating that they both lead second-phase [$Ca^{2+}$] dynamics. However, further analysis showed
122 significant difference between these two cell states: leader cells had much earlier calcium wave
123 (greater negative phase lag) compared to the first responder cells (p=0.0109). Thus, based on the
124 first- and second-phase [$Ca^{2+}$] dynamic metrics, first responder cells were distinct from the leader
125 cells.

126 Comparing coordination of [$Ca^{2+}$] wave during the second-phase [$Ca^{2+}$] response to
127 glucose, we found that first responder and leader cells were not different from the islet-average
128 (Fig.1 H), unlike hub-like(ph2) cells which showed a significantly higher number of links
129 compared to the islet average (p=0.0018). Thus, first responder cells are distinct from previously
130 defined hub cells. Extended analysis of the features of the [$Ca^{2+}$] dynamics (including network
131 analysis revealing hub-like cells in the first-phase [$Ca^{2+}$]) is presented in Fig.S1 E-K.

132 We next looked at the spatial organization of the first-phase [$Ca^{2+}$] response to glucose.
133 Distances between different β-cells were measured in a z-plane ~10-20 μm away from the surface

134 of the islet's beta-cell core. (Fig.1A). Distances were measured from each first responder cell in
135 the islet and then averaged (see Fig.1 I, J and methods). First responder cells formed clusters of
136 size <20μm (Fig.1 J red bar). The first responder clusters were significantly spatially separated
137 from leader cells (p=0.0208) and from hub-like(ph2) cells (p=0.0056). On average first responder
138 cells were located <30μm away from leader cells, and 45 μm from hub-like(ph2) cells (Fig.1 J).
139 The response time of β-cells in the islet following glucose stimulation was generally dependent on
140 their relative proximity to a first responder cell, where cells closer to first responder cells responded
141 earlier (Fig.S2 A). A linear dependence of the response time vs proximity of the first responder
142 was clear for some islets. For other islets location of the first responder cells was such that multiple
143 response domains with a local first responder in the center were formed (examples are shown in
144 Fig.S2 B). We defined the speed of the response propagation as the slopes of the distance to first
145 responder vs the time of response (Fig.S2 A). This time over which the initial response to glucose
146 response propagated across the islet was measured here for the first time, and it varied substantially
147 from islet to islet between 0.16 and 3.3 μm/sec. Given different islets had substantially different
148 rates of response to glucose we subsequently normalized the response time by islet.
149

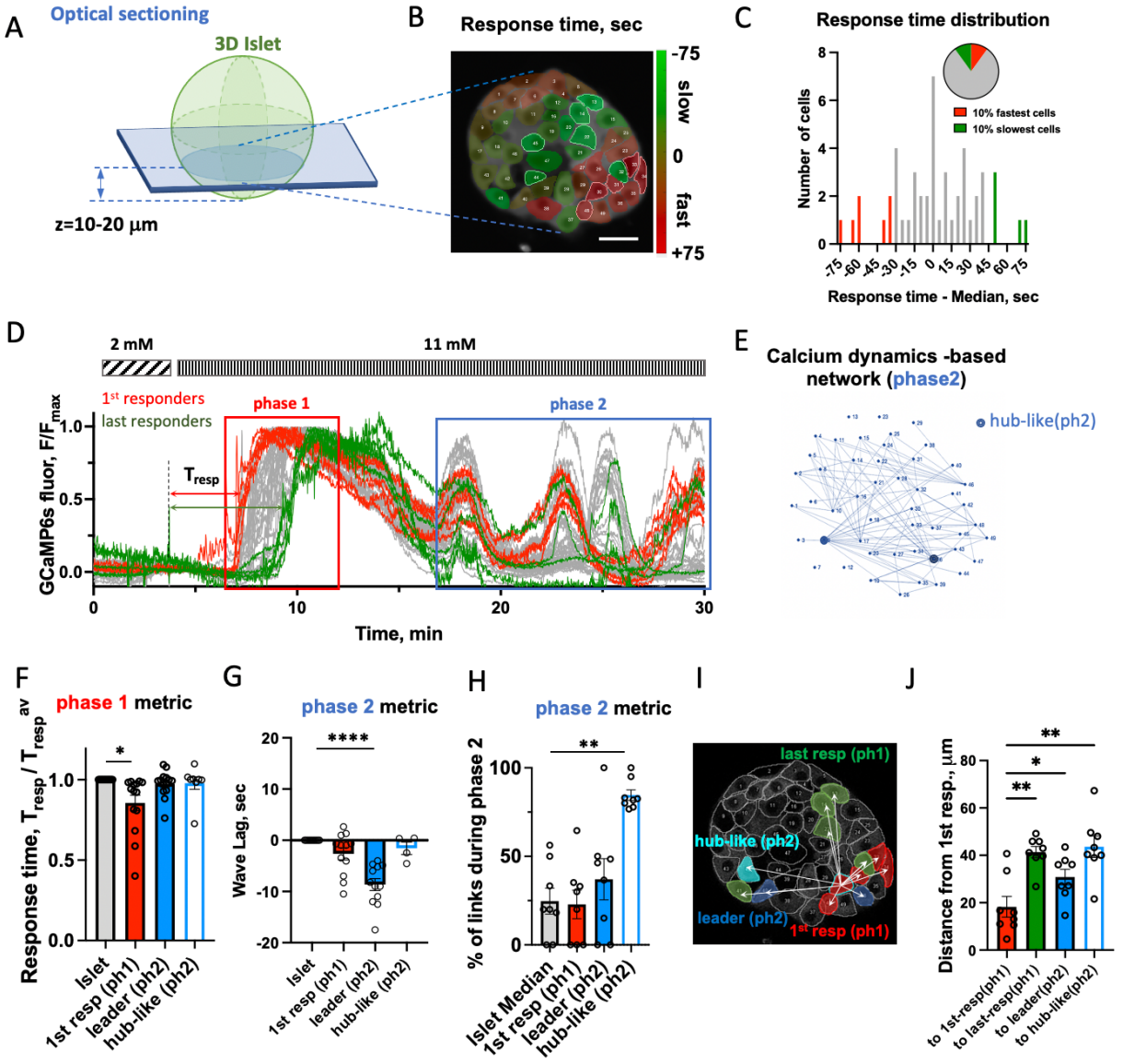


**Figure 1. Identification of first responder cells. A)** Schematic of where data was collected. **B)** Representative image of 2D islet plane with false-color map of response time to glucose elevation. **C)** Representative distribution of response time, Tresp, for the cells shown in (B). Pie chart describes definition of 1st (last) responder cells as 10% of all cells in the islet 2D plane which have fastest (slowest) Tresp. **D)** Representative time-course of $[Ca^{2+}]$ dynamics within an islet shown in (B) following glucose elevation from 2 to 11 mM. In red rectangle: first-phase of the $[Ca^{2+}]$ response, in blue – second phase. Red curves correspond to first responder (1st-resp) cells, and green – to last responder (last-resp) cells. **E)** Link map based on the functional network analysis performed over the second phase dynamics in the islet shown in (B and E). Hub-like (ph2) cells are shown as blue dots. **F)** Phase1 $[Ca^{2+}]$ dynamics metric: response time following glucose elevation. Comparison of β-cells leading phase1 (1st responder ph1) vs phase2 (leader ph2), vs hub-like (ph2) cells collected from 8-12 islets, 6-7 mice. **G)** Phase2 $[Ca^{2+}]$ dynamics metric: lag of the cell's $[Ca^{2+}]$ wave with respect to the islet-average wave. Comparison of β-cells leading phase1 vs phase2 vs hub-like (ph2) cells (n=4-12 islets from 4-7 mice). **H)** Percent of functional links normalized to max number of links, identified during second phase of $[Ca^{2+}]$ dynamics (n=8 islets from 6 mice). **I)** Example of measurement of the distance from one of the 5 first responder cells in this islet to other cells. **J)** Quantification for multiple islets (n=8 islets from 6 mice), where each dot represents average distance from all first responder cells to other cell states per islet. Statistical analysis in F, G utilized one sample t test, H, J: utilized One-way ANOVA (with multiple comparison post-hoc test) where **** represents $p<0.0001$, *** $p<0.0002$, ** $p<0.0021$, * $p<0.0332$ for comparison of the islet-average value vs all other

168 groups. Functional network analysis was performed via binarization and co-activity matrix analysis, as described [20].
169 See Figure 1 - Source Data for values used in each graph.
170

171 *Clusters of first responders are spatially consistent.* We reasoned that if cells respond randomly to
172 glucose stimulation, then first responder cells identified during the initial glucose elevation will
173 not be the same first responder cells during a repeated glucose elevation. Conversely if there exists
174 a functional hierarchy of cells within the islet, then there should be consistency in the location of
175 the first responder cells. We first stimulated islets to elevated (11 mM) glucose, lowered back to
176 basal levels, and re-stimulated over the course of 1-2 h (Fig.2 A). The location of the first responder
177 cluster in the islet remained consistent between the initial and repeated glucose elevation (Fig.2 B,
178 C). Some initial first responder cells were first responders in the repeated glucose stimulation (35%
179 of cases), whereas some surrendered their role either to the nearest neighbor cell (35%), or to the
180 2nd neighbor (18%), or to a more distant cell (12%).

181 We examined location of the first- and last responder cells, as well as leader cells in 3-
182 dimensions (Fig. S3). Within three cell layers, each separated by 10 μm, the locations of each β-
183 cell subpopulation were conserved, suggesting functional organization in 3-dimensions, as we
184 observed in 2-dimensions.
185

186 *Temporal consistency of first responder cells in not rigid.* We next sought to determine whether
187 an early response time was a consistent feature of first responder cells. As above, we first
188 stimulated islets to elevated (11 mM) glucose, lowered back to basal levels, and re-stimulated over
189 the course of 1-2 h (Fig.2 A). The period of the observed slow oscillations was in the same range
190 as previously reported [37], (T=246±89 sec, Fig.S4 A). No significant difference was observed in
191 the frequency of the oscillations during the repeated stimulation (0.011±0.008 Hz vs 0.007±0.001

192 Hz, Fig.S4 B). Response times for all cells during the initial and repeated glucose stimulation are
193 shown in Fig.S4 C for individual islets. When considering all cells within the islet, there was no
194 significant correlation between the response time of a cell during the initial stimulation compared
195 to the response time upon the repeated stimulation. However, first responder cells in the majority
196 of islets still remained consistent, while last responder cells were not consistent (Fig.S4 C). We
197 found that temporal consistency of *first responder* cells (Fig.2 D) was substantial, but not fully
198 rigid. Upon re-stimulation, the initial first responders retained a response that was significantly
199 earlier than the median islet response time: on average in the fastest 25% of the whole $T_{resp}$
200 distribution. In contrast, the last-responding cells lacked consistency upon repeated glucose
201 elevation, with a response time close to the islet-average (Fig.2 E).

202 To test whether first responder cells are maintained over a longer time, we measured the
203 response time upon elevated glucose within the same cell layer in the islet for 48 h at 6 h intervals.
204 At each time point we defined the first responder and last responder cells (Fig.2 F). There was no
205 significant difference in the total [$Ca^{2+}$] influx in the islet at each time point (Fig.2 G). The first
206 responder cells remained consistent during the first 12 hours, where they showed significantly
207 earlier [$Ca^{2+}$] response time than the islet average. However, at 18-24 h the first responder cells
208 became less distinguishable from the islet average, and at >24 h, their response time was
209 indistinguishable from the islet-average (Fig.2 H). A similar temporal pattern was observed for the
210 last responder cells (Fig.2 I). Thus, not all β-cells responded randomly to glucose stimulation.
211 Rather, a first responder β-cell state consistently led this response, but this was maintained only
212 over a ~24h time period.

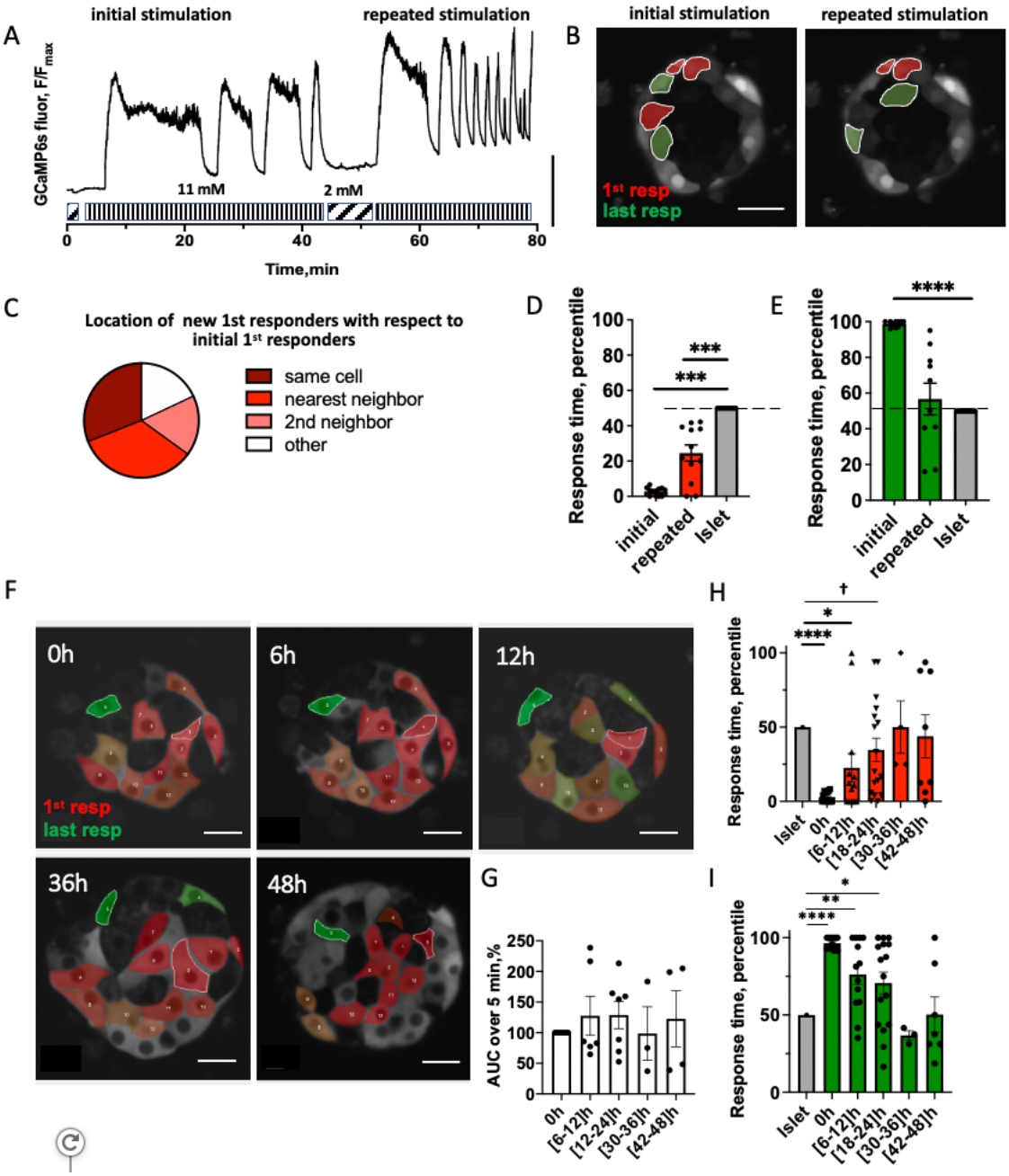


**Figure 2. Consistency of first responder cells.** A) Representative time-course of [$Ca^{2+}$] dynamics within an islet under repeated glucose stimulation. Vertical scale bar represents 30% of the fluorescence intensity change. B) Representative image of the islet with the location of first responders (red) and last responders (green) during initial and repeated glucose elevation. C) Spatial consistency: Spatial location of new first responder cells (during repeated glucose elevation) relative to the old first responder cells (during original elevation) (n=10 islets from 4 mice). D) time of response of cells identified as first responders during the initial glucose elevation and upon repeated glucose elevation (n=10 islets from 4 mice). E) As in D for last responders. F) False-color map indicating [$Ca^{2+}$] response time to glucose elevation during the first phase, recorded in the same region of the islet over 48 hours at 6 hour intervals. Scale bar indicates 20 µm. G) Area under the curve for [$Ca^{2+}$] elevation over 0-5 min for the islet average, for each time-window indicated. Data is normalized to the [$Ca^{2+}$] AUC at 0h. H) time evolution of the response time of the cells identified as first and I) As in H for last responders (n=7 islets from 3 mice). Statistical analysis in D, E utilized

one-sample t-test (with the null hypothesis of initial or repeated difference from the islet being 0). H, I utilized LMEM. † in H indicates p=0.06. See Figure 2 - Source Data for values used in each graph and Statistical Analysis – Source data for LMEM and one sample t-test details.

*First responder cells show characteristics of more excitable cells.* β-cells that have been previously identified to disproportionately recruit or maintain elevated [$Ca^{2+}$] in neighboring cells have shown elevated excitability, such as arising from increased metabolic activity [22]. We next examined characteristics of the first responder cells that may allow them to show an earlier response time. We first tested whether first responder cells have differing regulation of resting membrane potential (for example, a lower $K_{ATP}$ conductance or increased depolarizing current) that would increase the likelihood of earlier membrane depolarization in response to glucose elevation. We performed sequential glucose and glibenclamide stimulation, in the same manner as repeated glucose stimulation experiments. Following each stimulation, we identified first responder cells (Fig.3 A). Those cells which responded first to glucose, also showed a significantly lower than average response time to glibenclamide (Fig.3 B, C) (p=0.046). In contrast, those cells which responded last to glucose, did not show a response time different to the islet average under glibenclamide (Fig.3 D). When all cells in the islet plane were considered, we did not observe a significant correlation between the response time during glucose stimulation as compared to the response time upon glibenclamide stimulation. This suggested that while differing $K_{ATP}$ conductance (or resting depolarizing current) may be one factor in defining the earlier response time for a *first responder cell*, other factors are also likely involved.

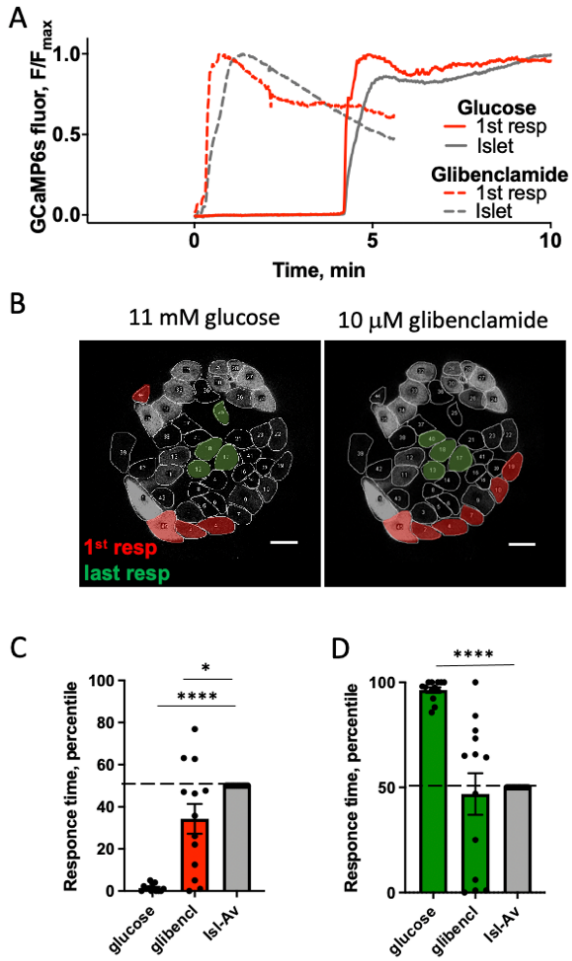


**Figure 3. Responsiveness of first responder cells to secretagogues**. A) Representative time-course of [$Ca^{2+}$] dynamics within an islet under 11 mM glucose stimulation (dashed curve) and under 10 μM glibenclamide (solid curve) stimulation for first responder cell (red) and islet-average (grey). B) Representative image of the islet with the location of first responders (red) and last responders (green) during glucose and glibenclamide stimulation. Scale bar indicates 20 μm. C) time of response of cells identified as first responders during glucose stimulation and upon glibenclamide stimulation (n=13 islets from 7 mice). D) As in C for last responder cells. Statistical analysis in C, D utilized one-sample t-test (with the null hypothesis of glucose or glibenclamide difference from the islet being 0). See Figure 3 - Source Data for values used in each graph.

To discover other factors that may characterize first responder cells, we examined the [$Ca^{2+}$] influx upon glucose stimulation (Fig.4 A). First responder cells demonstrated significantly higher influx of [$Ca^{2+}$] during the first-phase [$Ca^{2+}$] response (p=0.0072), while last responder cells had significantly lower [$Ca^{2+}$] influx (p=0.453) (Fig.4 B, C). First responder cells did not have a greater than average NAD(P)H levels at either low (2 mM) or elevated (11 mM) glucose (Fig.4 D, E). Interestingly, following dye transfer kinetics via FRAP first responder cells showed lower than average gap junction permeability (p=0.0270) (Fig.4 F, G).

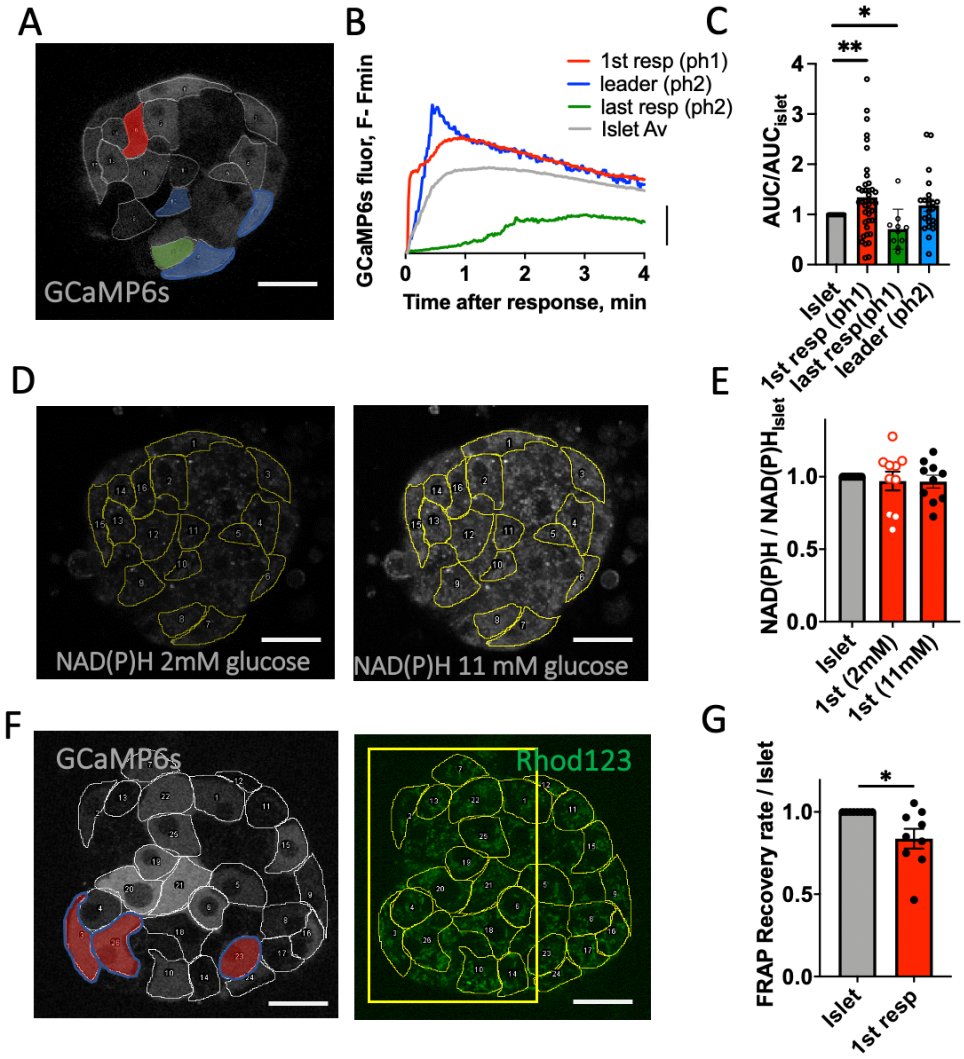


**Figure 4. Characteristics of first responder cells.** A) Representative image of the islet with first responders (red), leader (blue) and last responder (green) indicated. B) Time course of [$Ca^{2+}$] elevation in each cell population, indicating Area under the curve. C) Area under the curve for each cell state during the first 3 min after [$Ca^{2+}$] elevation upon elevated glucose (16 islets from 9 mice). D) Representative image of NAD(P)H autofluorescence in islet indicated in A, at low (2 mM) and high (11 mM) glucose. E) Mean NAD(P)H intensity in each identified subpopulation of β-cell, at low (2 mM) and high (11 mM) glucose, normalized with respect to the islet average (n=10 islets from 10 mice); F) Reprehensive GCamP6s fluorescence and Rhodamine123 fluorescence (for FRAP measurements) within the same islet layer. G) Mean Rhodamine123 fluorescence recovery rate as calculated during FRAP (n=7 islets from 5 mice). Scale bar indicates 20 µm. Statistical analysis in C utilized one-sample t-test where **** represents $p<0.0001$, *** $p<0.0002$, ** $p<0.0021$, * $p<0.0332$ for comparison of the islet-average value vs all other groups. In E, G utilized one-sample t-test (with the null hypothesis of 1$^{st}$ responder difference from the islet being 0) where * $p<0.05$ indicated comparing the islet-average value vs first responder group. See Figure 4 - Source Data for values used in each graph.

*First responder cells drive first-phase [$Ca^{2+}$] elevation.* To test whether the hierarchy of cell responsiveness is functionally important, and specifically whether the earliest responding cells disproportionally drive the islet [$Ca^{2+}$] response, we removed single β-cells from the islet via two-

295 photon induced femtosecond laser ablation. Two-photon laser ablation allows for highly targeted
296 removal of a cell without disrupting cells in close proximity [33]. As previously, we measured
297 [$Ca^{2+}$] dynamics upon elevation from 2 mM to 11 mM glucose; lowered glucose back to 2 mM,
298 ablated one cell, and then repeated glucose elevation (Fig.5 A). Under each glucose elevation we
299 identified first responder cells (Fig.5 B). Upon ablation of a control (non- first responder) cell the
300 islet [$Ca^{2+}$] response was relatively unchanged, with robust second-phase [$Ca^{2+}$] oscillations (Fig.5
301 A, B). Upon ablation of a first responder cell robust second-phase [$Ca^{2+}$] oscillations were also
302 observed (Fig.5 C). And a new cell within the islet becomes the first responder cell (Fig.5 D).

303 We examined the [$Ca^{2+}$] response timing and [$Ca^{2+}$] elevation in cells across the islet during
304 the first-phase [$Ca^{2+}$] response to glucose following ablation of either control (non- first responder)
305 cell or first responder cell. Following ablation of the control cell, the response time of first
306 responder cells remained below the islet-average (Fig.5 E, p=0.0022); whereas last responder cells
307 were not different from the islet average (Fig.5 F). On average 53% of the original first responder
308 cells remained as the earliest responding cells (Fig.S5 A center). These findings are very similar
309 to those in the absence of any cell ablation (Fig.S5 A left). Following ablation of a first responder
310 cell, the response time of the next earliest responder cells remained below the islet-average (Fig.5
311 H, p=0.0019); whereas last responder cells again were not different from the islet average (Fig.5
312 I). On average 40% of the original next earliest responding cells ('second responder' cells) become
313 new earliest-responding cells (Fig.54 A right) and in another 20% of cases they remained as second
314 responder cells. This suggests a hierarchy in the timing and β-cell responsiveness to glucose.

315 We next quantified the effect of a cell ablation on the whole islet first-phase [$Ca^{2+}$]
316 response. We first defined the [$Ca^{2+}$] influx as the area under the curve for [$Ca^{2+}$] over 5 min
317 following elevation (Fig.5 K). We observed a size-dependence in area under the curve in both

318 control and first responder ablation cell experiments (Fig.S5 B), hence we separated islets into
319 small and large islets based on the median of the size distribution (Fig.S5 C). In large islets
320 (>89 μm diameter) the islet-average [$Ca^{2+}$] influx was not different between control or first
321 responder cell ablation cases (Fig.5 J). In small islets (<89 μm diameter) while the islet-average
322 [$Ca^{2+}$] influx decreased following ablation of each cell type, the decrease was significantly greater
323 following ablation of first responder cells. Consistent with these observations the proportion of
324 cells that showed elevated first-phase [$Ca^{2+}$] (i.e. within 5 min. of [$Ca^{2+}$] elevation) was largely
325 unchanged in large islets, with 93% of cells showing elevated [$Ca^{2+}$] for ablation of both first
326 responder or control cells (Fig.5 K). In small islets the proportion of cells that showed elevated
327 first-phase [$Ca^{2+}$] was largely unchanged following control cell ablation (91% of cells), but
328 substantially decreased following first responder cell ablation (42% of cells). A similar trend was
329 observed in terms of connectivity during the first-phase [$Ca^{2+}$] elevation: the mean number of
330 functional links within the islet was significantly less following first responder cell ablation
331 compared to the control cell ablation (Fig.5 L). Finally, we measured the response time of the islet
332 following ablation of a first-responder cell (Fig.5 M, N). We did not observe significant changes
333 in large islets under ablation of a first responder cell, control cell or with no ablation. Similarly,
334 we did not observe significant change in small islets under ablation of a control cell or with no
335 ablation. However, following ablation of a first responder cell, the time for a [$Ca^{2+}$] response of an
336 islet significantly increased (Fig.5 M, N). Thus, in smaller islets, removal of a first responder cell
337 via femtosecond laser ablation diminishes and delays the elevation of first-phase [$Ca^{2+}$] as a result
338 of there being fewer cells that respond both rapidly and in a coordinated fashion.

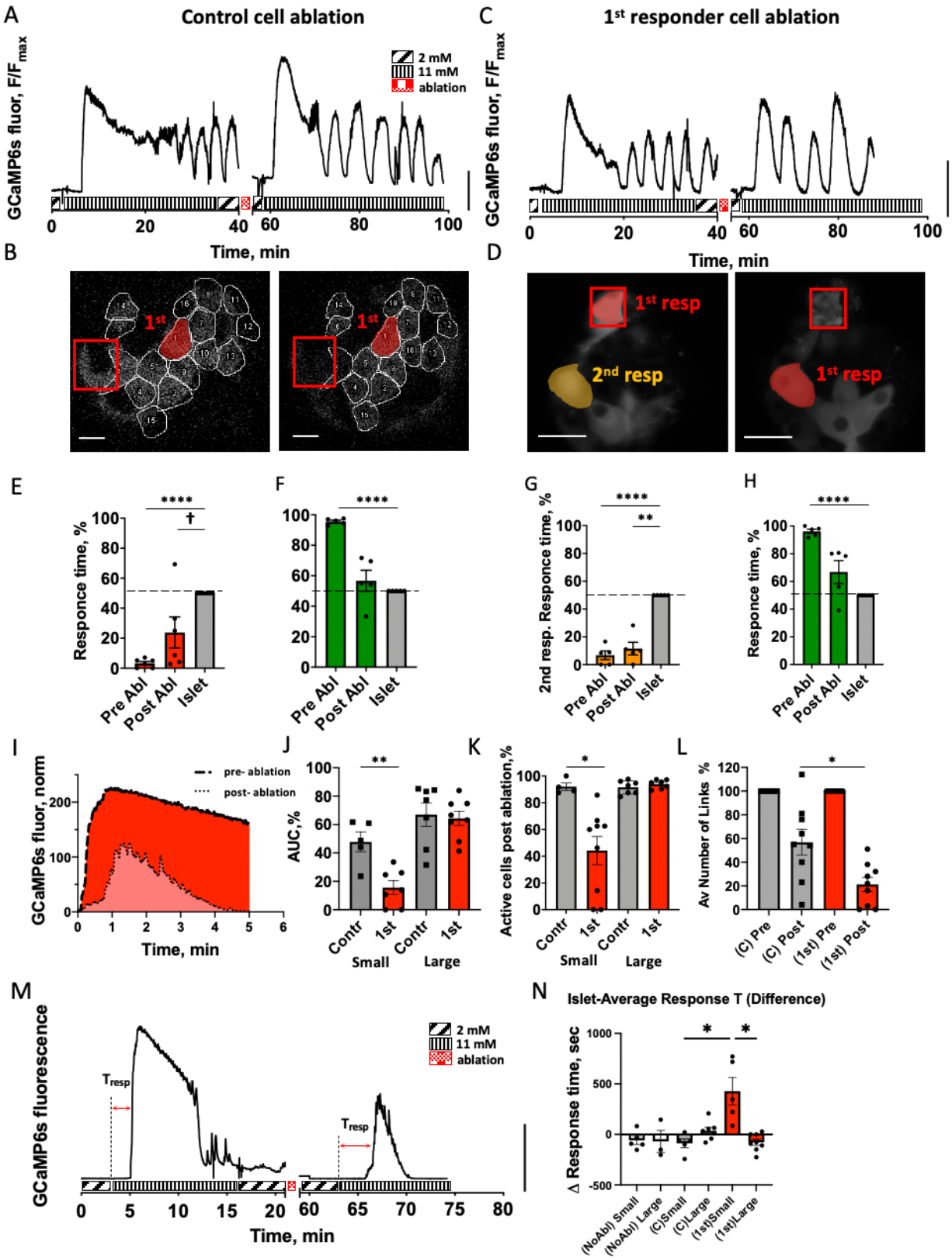


**Figure 5. Role of first responder cells. A)** Representative time-course of [$Ca^{2+}$] dynamics within an islet pre- and post- ablation of a control cell (non-first responder cell). Vertical scale indicates 30% fluorescence intensity change.

**B)** Representative image of the islet with the location of first responders (red) pre- and post- ablation of a control cell (red square). **C)** As in A for ablation of first responder cell. **D)** As in B for ablation of first responder cell (Red square), with second responder cell highlighted (orange). **E)** time of response of cells identified as first responders prior to control cell ablation and following control cell ablation (n=6 islets from 6 mice). **F)** As in E for last responders. **G)** Time of response of cells identified as second responders prior to first responder cell ablation and following first responder cell ablation (n=5 islets from 5 mice). **H)** As in G for last responders. **I)** Representative time course of $Ca^{2+}$ elevation following glucose elevation pre- and post- ablation, with the Area-Under-the-Curve indicated. **J)** Area-Under-the-Curve for the first-phase [$Ca^{2+}$] response post ablation of a control and first responder cells, for small (<89 μm diameter) and large (>89 μm diameter) islets. Data is normalized to the Area-Under-the-Curve prior to ablation. (27 islets from 17 mice) **K)** % of cells that show [$Ca^{2+}$] elevation post ablation of a control and first responder cells, for small and large islets. Data is normalized to the Area-Under-the-Curve prior to ablation; **L)** Average number of functional links per islet during the first-phase of [$Ca^{2+}$] response for a control and first responder cell ablations, for small and large islets combined. Data is normalized to the number of functional links prior to ablation (n=9 islets for each group). Functional network analysis was performed via Pearson-product algorithm, as described before [21]. **M)** Representative [$Ca^{2+}$] pre- and post- first responder ablation in a small islet, Tresp indicates islet-average response time. **N)** Response time change in case of no ablation (white bars), control cell ablation (grey bars), or first responder cell ablation (red bars) (35 islets from 20 mice). 2 small islets that underwent first responder cell ablation did not respond at all following ablation and were excluded from analysis due to "infinite" response time post-ablation. Statistical analysis in E, F, G, H utilized one-sample t-test (with the null hypothesis of pre-or post- difference from the islet being 0) where **** represents $p<0.0001$, *** $p<0.001$, ** $p<0.01$, * $p<0.05$ indicated for comparison of the groups. † in (E) indicates significance of $p=0.06$. In I, J, K, L utilized ANOVA with multiple comparison Kruskal-Wallis test, where * $p<0.0332$ comparing the groups indicated. See Source Data – Figure 5 and Statistical analysis files for values used in each graph.

*Computer model description of first responder cell characteristics.* To understand which characteristics of first responder cells are required for their action we utilized a previously published multi-cell model of islet β-cell electrophysiology [34]. This model incorporates heterogeneity in multiple metabolic, electrical and gap junctional characteristics. We simulated the [$Ca^{2+}$] response upon elevated glucose (Fig.6 A) and observed significant variability in the time of [$Ca^{2+}$] elevation (Fig.6 B). We defined first responders as the 10% of all cells with the fastest response times, as in experiments. We first examined the characteristics of these first responder cells in the model islet. The rate of glycolysis for model first responder cells was not significantly different from the islet-average (Fig.6 C), consistent with NAD(P)H measurements. The open channel $K_{ATP}$ conductance (equivalent to channel number) for model first responder cells was significantly lower than the islet-average (Fig.6 D), in agreement with the earlier-than average response time under glibenclamide stimulation. The coupling conductance for model first responder cells was slightly, but significantly lower than the islet average (Fig6 E), consistent with

379 gap junction permeability FRAP experiments. Model last responder cells showed no difference in
380 glycolysis rate, elevated $K_{ATP}$ conductance and reduced coupling conductance (Fig.6 C-E). Thus,
381 model first responder cells are characterized by a combination of both lower electrical coupling
382 and higher membrane excitability because of lower $K_{ATP}$ conductance; whereas model last
383 responder cells are characterized by a combination of both lower electrical coupling and lower
384 membrane excitability because of greater $K_{ATP}$ conductance.

385 To investigate the relative role of these functional characteristics and to define first
386 responder cells, we simulated the [$Ca^{2+}$] response following each of the above-mentioned
387 parameters being *adjusted* to be equal to the corresponding islet-average parameter (Fig.6 F-H):
388 little change in glycolysis rate, increase in $K_{ATP}$ conductance or increase in coupling conductance.
389 Thus, if a specific parameter is necessary for the function of the first responder, adjusting that
390 parameter would be expected to significantly change the response time of that cell. Of the three
391 parameters examined, re-adjusting the $K_{ATP}$ conductance had the greatest impact on the first
392 responder cell response time (Fig.6 I) and whether a first responder cell retained the earliest [$Ca^{2+}$]
393 elevation (Fig. 6J). In addition, rearrangement of the cell position within the islet, and thus the
394 neighboring cells in contact with the first responder cell, significantly disrupted whether a first
395 responder cell showed the earliest elevation in [$Ca^{2+}$] (Fig. 6K). Thus, model first responder cells
396 are defined by both increased excitability and position within the islet.

397 Finally, we tested whether first responder cells acting via gap junction coupling were
398 sufficient to recruit neighboring cells. Following simulation of the islet, we removed either a
399 random set of control cells or the earliest responding cells and re-simulated the islet [$Ca^{2+}$]
400 response. Consistent with experimental measurements, removal of first responder cells diminished
401 the area under the curve for the islet-average [$Ca^{2+}$] elevation, whereas removing a control set of

402 cells had no impact on the islet-average [$Ca^{2+}$] elevation (Fig.6 L). Importantly a decrease in [$Ca^{2+}$]

403 elevation was only observed for removal of greater than 10% of the earliest-responding cells; with

404 greater reduction for removal of a higher % of cells. Thus, gap junction coupling is sufficient for

405 a population of first responder cells to exert control over first phase [$Ca^{2+}$] in the islet.

406

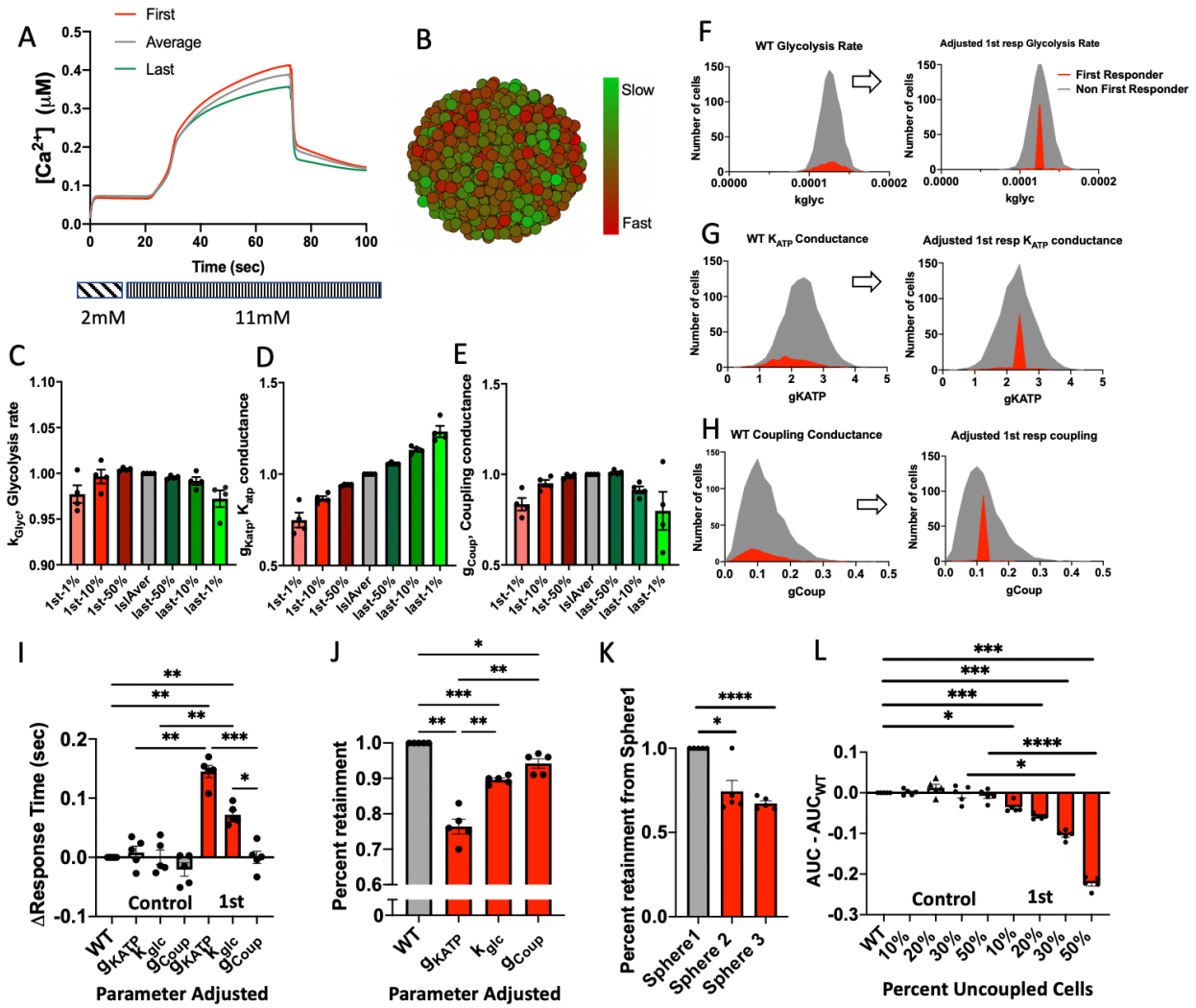


407

408 **Figure 6. Modelling first responder cells.** A) Representative time-course of [$Ca^{2+}$] in a simulated islet, indicating
409 the [$Ca^{2+}$] dynamics characterizing the first responder ($1^{st}$-resp) and last responder (last-resp) cells compared to the
410 islet-average. B) False-color map indicating [$Ca^{2+}$] response time to glucose elevation during the first phase. C) Mean
411 parameter value of glycolysis rate ($k_{glyc}$) averaged over the first (red) and last (green) indicated % of responding cells
412 (n=4 seeds). Data is normalized with respect to the islet average parameter. D) As in C for $K_{ATP}$ conductance ($g_{KATP}$).
413 E) As in C for coupling conductance ($g_{coup}$). F) Distribution of the glycolysis rate ($k_{glyc}$) in non-first responders (grey)
414 and first responders (red) before (left) and after (right) parameter adjustment to set first responder parameter the same
415 to the islet average value (n=5 seeds). G) As in F for adjustment of $K_{ATP}$ conductance ($g_{KATP}$). H) As in F for adjustment

of coupling conductance ($g_{coup}$). I) Change in response time upon adjustment of the glycolysis rate ($k_{glyc}$), $K_{ATP}$ conductance ($g_{KATP}$) and coupling conductance ($g_{coup}$) in first responder indicated in F-H, or in a random sub-set of cells. J) Percent of the original first responder cells that remain among the earliest responders after adjustment of adjustment of $k_{glyc}$, $g_{KATP}$, $g_{coup}$ in first responder cells indicated in F-H. K) Percent of the original first responders that remain among the earliest responders after adjustment of the spatial position of the first responders in three separate distributions (spheres) (n=5 seeds). L) Decrease in the Area-Under-the-Curve (AUC) of the first phase of the $Ca^{2+}$ response following de-coupling (removal) of a given % of the first responder or a random set of cells from the islet (n=5 seeds). Statistical analysis in I, J, K, L utilized one-way ANOVA (with Multiple comparison post-hoc test) where **** represents $p<0.0001$, *** $p<0.001$, ** $p<0.01$, * $p<0.05$ comparing he groups indicated. See Figure 5 - Source Data for values used in each graph.

427 **Discussion**

428 β-cells within the islet are functionally heterogeneous. While subpopulations of β-cells have been
429 suggested to maintain coordinated oscillatory [$Ca^{2+}$] and insulin release [35], these are associated
430 with the second phase of the [$Ca^{2+}$] response; a point at which cell-cell electrical communication
431 is less important for *recruiting* [$Ca^{2+}$] and the level of insulin release, but is critically important for
432 *coordinating* pulsatile [$Ca^{2+}$] and insulin secretion dynamics. Given the importance of cell-cell
433 electrical communication in regulating first-phase insulin release [16], we examined whether there
434 exists a subpopulation of β-cells associated with the first-phase calcium response. We discovered
435 a functional cell state that we termed "first responder". First responder cells lead the first-phase
436 [$Ca^{2+}$] response, and were distinct from previously identified functional subpopulations of β-cells.
437 These cells were more excitable, critical for recruiting β-cells to elevate [$Ca^{2+}$] immediately
438 following glucose stimulation (Fig.7). We further demonstrated that this state of the β-cell is
439 conserved over a ~24 h time period.

440

441 *First responder cells represent a distinct functional state of the* β-*cell*:

442 We defined first responder cells as those β-cells that lead the first-phase [$Ca^{2+}$] response, more
443 specifically the 10% of cells in the islet with the earliest response time. Importantly upon repeated
444 stimulation, the same cells generally showed an earlier-than-average response over 1-2 hours
445 (Fig.2), unlike last responder cells, which lacked any consistency. Only in ~50% of the islets initial
446 first responder cells remained consistent during repeated glucose elevation (Fig.S5 A). Therefore,
447 the temporal consistency of this cell state is not rigid. Some of them surrendered their first
448 responder role either to a nearest neighbor cell, or to a 2$^{nd}$ nearest neighbor. Therefore, the spatial
449 location of the first responder cluster remained consistent (Fig.2 E).

450 We demonstrated that first responder cells are distinct from other functional subpopulations
451 of β-cells previously defined by [$Ca^{2+}$] signatures. Leader (wave-origin) sells have been associated
452 with regulating second phase [$Ca^{2+}$] dynamics [22, 23]. Hub cells have been associated with
453 maintaining elevated, coordinated [$Ca^{2+}$]. Thus, the heterogeneity that controls second-phase
454 [$Ca^{2+}$] is different than the first-phase [$Ca^{2+}$]. We do note that hub cells were previously identified
455 following more rapid measurements of [$Ca^{2+}$] dynamics (~10fps) than in our study here (~1fps)
456 [20]. The lack of fast (<1s) timescale [$Ca^{2+}$] dynamics in our analysis may therefore exclude some
457 hub cells and mean that the hub-like (ph2) cells we identify are not exactly analogous to those
458 previously identified.

459 While the first-responder cells remained in the lead over 1-2 h, this consistency was
460 gradually lost after 24h (Fig.2). The overall responsiveness of the islet was maintained
461 (demonstrated by calcium influx, Fig2. G), indicating the loss of state is not simply due to islet
462 dysfunction. This finding suggests that first responder cells represent a transient functional state
463 of the islet and not a permanent subpopulation of the β-cell. We are not aware of other long-term
464 imaging studies beyond 1-2 h that test whether functional subpopulations represent transient states
465 of the β-cell rather than permanent β-cell subpopulations. The current lack of genetic markers for
466 first responder cells hinders robust lineage tracing approaches to validate this finding. Indeed, this
467 first-responder cell state may represent a sub-set of the more mature functional cell subpopulations
468 that have been genetically marked [2]. Cyclic expression of *Ins2* gene activity has been reported
469 in subsets of β-cells [36], suggesting that transient states of the β-cell can exist. A correlation
470 between *Ins* expression and *GJD2* (coding Cx36) expression has also been demonstrated [37].

471 Thus, we speculate that fluctuations in Cx36 expression may contribute to first responder
472 cells: increases in Cx36 gap junction conductance would suppress first responder cells as a result

473 of hyper-polarization by less excitable neighboring cells. Decreases in Cx36 gap junction
474 conductance (as is observed in first responder cells, Fig.4) would allow the more excitable first
475 responder cells to respond earlier and impact their neighboring cells. Decreased gap junction
476 conductance would prevent a cell being hyper-polarized and inhibited by less excitable
477 neighboring cells. Our computational model of the islet also showed lower gap junction
478 conductance within the first responder cells. However, we cannot exclude a role for intra-islet
479 paracrine factors in also regulating first responder cells.

480 An important consideration is that our study, along with other studies [20, 22], examines a
481 single plane of cells within the islet. Thus, the first responder cells are relative to that islet region.
482 It is quite likely that elsewhere in the islet at other planes, cells that respond earlier are present
483 which may play a more important role. Nevertheless, first responder cells represent a distinct
484 functional state of the β-cell, stable for ~24 hours, and regulating the first phase of [$Ca^{2+}$] and
485 likely also insulin secretion.

486

487 *First responder cells represent a more excitable subpopulation:*

488 We hypothesized and demonstrated that first responder cells are important to recruit elevated
489 [$Ca^{2+}$] in neighboring cells. Previously we identified highly-excitable cells that effectively
490 recruited elevated [$Ca^{2+}$] in neighboring cells [22]. These cells showed increased NAD(P)H
491 responses. However, while first responder cells showed increased [$Ca^{2+}$] influx compared to
492 neighboring cells, they did not show any difference in NAD(P)H levels (Fig.4). First responder
493 cells however did show some level of consistency following glibeclamide stimulation that inhibits
494 $K_{ATP}$ channels (Fig.3), although not to the consistency found with glucose stimulation. First
495 responder cells likely show differences in ion channel composition, which may include reduced

496 $K_{ATP}$, but equally could include an increased resting depolarizing current (Fig.7A). For example,
497 increased expression of HCN channels has been found in a population of human beta-cells that is
498 important for increased insulin secretion [39]. The reduced correlation between glucose and
499 glibenclamide stimulation suggests that first responders are also defined by other factors.
500 Functional subpopulations (e.g 'hub cells', 'wave-origin' or 'leader') have been identified to show
501 differences in glucose metabolism [20, 22], which may also explain their distinction from first
502 responder cells.

503 Notably, we observed consistent results within our computational model of the islet (Fig.6).
504 In the model, first responder cells showed decreased $K_{ATP}$ conductance but little difference in GK
505 activity. Supporting this, disrupting $K_{ATP}$ conductance in the first responder cells led to other cells
506 responding earlier. Thus, first responder cells are likely more excitable due to altered ion channel
507 composition, although whether this is due to altered $K_{ATP}$ channel activity or other ion channels
508 (e.g. HCN channels) is still to be determined. We also observed in the model that the cell position
509 within the islet was important: rearranging the position of the first responder cells, and thus the
510 neighboring cells in contact with the first responder cells, disrupted their consistency. While
511 technically challenging, dissociation of islets post-first responder cell identification, and
512 association of islets into pseudo-islet structures would allow this property to be tested [40].
513 Nevertheless, we did observe that the first-phase response time is spatially organized within 2-3
514 cell layers. This further suggests spatial positioning, and thus the influence of neighboring cells
515 within this region, is important (Fig.7 C).

516 As such, first responder cells are more excitable cells, likely as a result of altered ion
517 channel composition, as well as partially decreased gap junction coupling, and/or spatial
518 positioning within the islet.

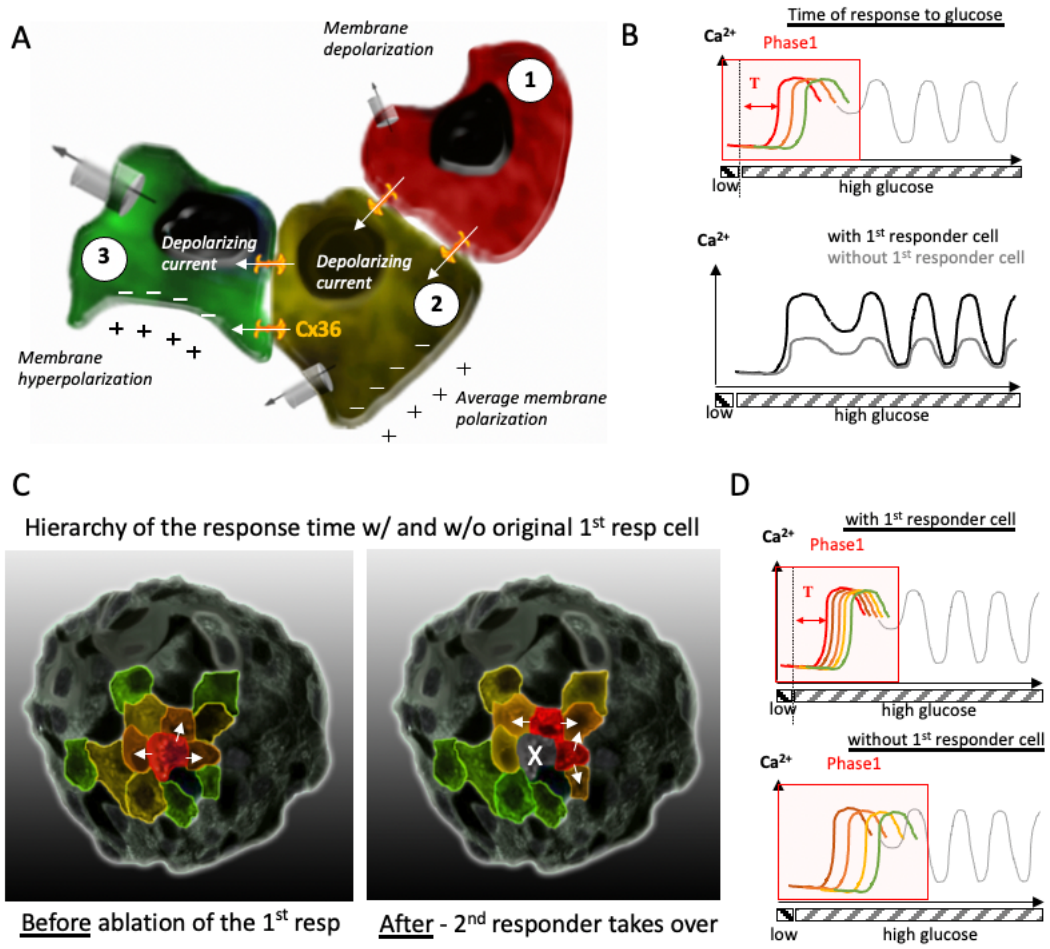


Figure 7

**Figure 7. Schematic representation of the role of first responder cells in the islet.** A) Cell1 - first responder cell (red) is more prone to membrane depolarization upon glucose stimulation. Cell 2 (yellow) is less depolarized than a first responder. The difference in the membrane potential between the cell 1 and 2 leads to depolarizing current to flow through the gap junctions into cell 2 triggering depolarization. Cell 2 subsequently depolarizes the less excitable cell 3 (green). B) Representation of the [$Ca^{2+}$] response to glucose in cells 1,2,3 shown in (A), and the islet-average [$Ca^{2+}$] response with (black) and without (grey) the first responder cell. C) Schematic of the time of response in the islet (red – faster response, green - slower) before and after the first responder ablation. Post-ablation, the cell with the second-earliest response time takes over the role of the first responder. D) Representation of the [$Ca^{2+}$] coordination before and dis-coordination after the first responder cell ablation.

*First responder cells drive first phase [$Ca^{2+}$] elevation*:

Following fs laser ablation of first responder cells we observed a decline in the first-phase [$Ca^{2+}$] response, in terms of the level of [$Ca^{2+}$] uptake, the numbers of cells showing elevated [$Ca^{2+}$], the

534 first-phase [$Ca^{2+}$] coordination and the time taken to show elevated [$Ca^{2+}$] (Fig.5), compared to
535 the laser ablation of the non-first responder (control) cell. This indicates that first responder cells
536 are necessary for both recruiting and coordinating elevated [$Ca^{2+}$] following glucose elevation. We
537 observed qualitatively similar results in the islet model after removal of first-responder cells: the
538 integrated [$Ca^{2+}$] elevation over the first phase was diminished (Fig.6). This indicates that gap
539 junction coupling is sufficient to mediate the impact of first responder cells over the islet first-
540 phase [$Ca^{2+}$] response to glucose.

541 During the second-phase of [$Ca^{2+}$] elevation post-ablation we still observed [$Ca^{2+}$]
542 oscillations. Combining this finding with our discovery that different cells leading different phases
543 of the [$Ca^{2+}$] response to glucose (first responders vs leader), we conclude that first responder cells
544 are more important for recruiting and coordinating [$Ca^{2+}$] during a specific time window, and not
545 for the long-term maintenance of [$Ca^{2+}$] elevation (Fig.7 D). Interestingly, this observation is
546 similar to the regulation of [$Ca^{2+}$] by Cx36 gap junction channels. At elevated glucose almost all
547 β-cells are capable of elevating [$Ca^{2+}$] and insulin release. However, some cells elevate [$Ca^{2+}$] and
548 insulin release more rapidly and some elevate more slowly, likely as a result of being more or less
549 excitable, respectively. As a result, while all cells elevate [$Ca^{2+}$], the differences in their timing
550 prevent a robust first-phase insulin release [16].

551 Furthermore, the islet responded more slowly upon ablation of first responder cells. This
552 indicated the ability of first responder cells to trigger earlier responses in neighboring cells, not
553 just homogenizing otherwise heterogeneous response times. We therefore suggest that the more
554 excitable first responder cells recruit less excitable cells to elevate [$Ca^{2+}$] in a more coordinated
555 uniform manner, to enhance first-phase [$Ca^{2+}$]. It is worth mentioning that in zebrafish islets, laser
556 ablation of those cells that lead the [$Ca^{2+}$] elevation in response to glucose also disproportionately

557 affected islet-average [$Ca^{2+}$] influx, as compared to laser ablation of control cells [24]. Zebrafish
558 islets in that study were comparable in size to the small mouse islets analyzed in our work. It is
559 possible that these zebrafish "leader" cells are analogous to the first responder cells in mouse islets
560 that we describe in this study.

561 While model results presented here indicated that gap junction coupling was sufficient for
562 10% of first responder cells to drive first-phase [$Ca^{2+}$], we do note that more substantial
563 diminishments of [$Ca^{2+}$] influx were observed when greater numbers of earlier responding cells
564 were removed. This suggests the existence of functional redundancy in the ability of earlier
565 responding cells to drive the first-phase [$Ca^{2+}$] elevation. Indeed, following ablation of a first
566 responding cell, the 'new' first responding cells were cells that responded earlier than average
567 prior to cell ablation. This further explains how larger islets were relatively resistant to destruction
568 of individual cells. In small islets the much greater impact on [$Ca^{2+}$] likely is a result of both the
569 greater % of the islet that has been disrupted, and that there are fewer earlier responding cells to
570 replace the function of the first responder cell. As noted elsewhere, by restricting our analysis to a
571 single plane, as with other functional subpopulation studies, we are also potentially excluding cells
572 that respond even earlier and would be expected to show greater impact in controlling the first
573 phase [$Ca^{2+}$]. As such future studies should focus on full 3D analysis encompassing the whole
574 islet. Measuring how loss of first responder cells impacts insulin release itself will also be
575 important to establish, particularly to establish whether changes in first-phase [$Ca^{2+}$] impact first-
576 phase insulin release.

577 *Summary:*

578 Several functional β-cell subpopulations have been identified that influence islet function, yet it is
579 currently unknown whether these subpopulations overlap and whether the mechanisms by which

580 they affect the islet function are the same. This understanding has been hindered by a lack of
581 standard procedures in identifying functional subpopulations (e.g. by standard analysis of [$Ca^{2+}$]
582 dynamics, optogenetic stimulation or silencing). Longer-term imaging to track the consistency and
583 state of functional subpopulations has also been missing. We combined high resolution confocal
584 microscopy in islets with β-cell specific [$Ca^{2+}$] sensor expression, together with targeted removal
585 of single cells via 2-photon laser ablation and standardized analysis of [$Ca^{2+}$] coordination. We
586 discovered a distinct functional β-cell state that was stable for ~24h. The state is characterized by
587 increased electrical excitability and slightly reduced gap junction permeability. This state did not
588 overlap with other previously identified functional subpopulations. We discovered organization of
589 the first-phase [$Ca^{2+}$] response and existence of hierarchy in this response where the second earliest
590 to response cell takes over the role of the first responder cell upon the first responder cell ablation.
591 Removal of first responder cells disproportionately disrupted the response time of the islet and
592 [$Ca^{2+}$] levels during the first phase following glucose elevation, compared to the control cell
593 removal in the size-matched islets. Thus, we have identified a cell state that is functionally
594 important to a first phase of calcium response to glucose in individual islets.
595

596 **Methods:**

597 *Animal care:* Male and female mice were used under protocols approved by the University of
598 Colorado Institutional Animal Care and Use Committee. β-cell-specific GCaMP6s expression (β-
599 GCaMP6s) was achieved through crossing a MIP-CreER (The Jackson Laboratory) and a
600 GCaMP6s line (The Jackson Laboratory). Genotype was verified through qPCR (Transetyx,
601 Memphis, TN). Mice were held in a temperature-controlled environment with a 12 h light/dark
602 cycle and given continuous access to food and water. CreER-mediated recombination was induced
603 by 5 daily doses of tamoxifen (50mg/kg bw in corn oil) delivered IP.

604

605 *Islet isolation and culture*: Islets were isolated from mice under ketamine/xylazine anesthesia (80
606 and 16 mg/kg) by collagenase delivery into the pancreas via injection into the bile duct. The
607 collagenase-inflated pancreas was surgically removed and digested. Islets were handpicked and
608 planted into the glass-bottom dishes (MatTek) using CellTak cell tissue adhesive (Sigma-Aldrich).
609 Islets were cultured in RPMI medium (Corning, Tewksbury, MA) containing 10% fetal bovine
610 serum, 100 U/mL penicillin, and 100 mg/mL streptomycin. Islets were incubated at 37C, 5% CO2
611 for 24-72 h before imaging.

612

613 *Imaging:* An hour prior to imaging nutrition media from the isolated islets was replaced by an
614 imaging solution (125 mM NaCl, 5.7 mM KCl, 2.5 mM CaCl2, 1.2 mM MgCl2, 10 mM HEPES,
615 and 0.1% BSA, pH 7.4) containing 2 mM glucose. During imaging the glucose level was raised to
616 11mM. Islets were imaged using either a LSM780 system (Carl Zeiss, Oberkochen, Germany)
617 with a 40x 1.2 NA objective or with an LSM800 system (Carl Zeiss) with 20x 0.8 NA
618 PlanApochromat objective or a 40x 1.2 NA objective, with samples held at 37C.

619 For [$Ca^{2+}$] measurements GCaMP6s fluorescence was excited using a 488-nm laser.
620 Images were acquired at 1 frame/s at 10-15 um depth from the bottom of the islet. Glucose was
621 elevated 3 minutes after the start of recording, unless stated otherwise.

622 NAD(P)H autofluorescence and [$Ca^{2+}$] dynamics were performed in the same z-position
623 within the islet. NADH(P)H autofluorescence was imaged under two-photon excitation using a
624 tunable mode-locked Ti:sapphire laser (Chameleon; Coherent, Santa Clara, CA) set to 710 nm.
625 Fluorescence emission was detected at 400–450 nm using the internal detector. Z-stacks of 6–7
626 images were acquired spanning a depth of 5 μm. First the NAD(P)H was recorded at 2 mM
627 glucose, then the [$Ca^{2+}$] dynamics was recorder at 2 mM and during transition to 11 mM glucose.
628 After the [$Ca^{2+}$] wave was established, the NAD(P)H was recorded at 11 mM glucose.

629 Cx36 gap junction permeability and [$Ca^{2+}$] dynamics were performed in the same z-
630 position within the islet, with gap junction permeability measured using fluorescence recovery
631 after photobleaching, as previously described [17]. After [$Ca^{2+}$] imaging, islets were loaded with
632 12 mM Rhodamine-123 for 30 min at 37C in imaging solution. Islets were then washed and FRAP
633 performed at 11mM glucose at room temperature. Rhodamine-123 was excited using a 488-nm
634 laser line, and fluorescence emission was detected at 500–580 nm. Three baseline images were
635 initially recorded. A region of interest was then photobleached achieving, on average, a 50%
636 decrease in fluorescence, and images were then acquired every 5-15 s for 15 min.

637

638 *Imaging long term [$Ca^{2+}$] dynamics*: The initial [$Ca^{2+}$] dynamics under glucose elevation from 2
639 to 11 mM at 0 hours was recorded. The dish was marked to indicate its orientation with respect to
640 the microscope stage, and the arrangement of islets was noted to facilitate islet localization in
641 subsequent imaging. After this first time point, imaging solution was replaced by the islet culture

642 media and the dish was kept in the incubator at 37C and 5% CO2 until the next time point. The
643 same cell layer in the islet was imaged at 6h intervals until 48h. For some islets intervals of 12 h
644 were recorded.
645
646 *Laser ablation:* Laser ablation was performed with two-photon tunable mode-locked Ti:sapphire
647 laser (Chameleon; Coherent, Santa Clara, CA) set to 750 nm. First [$Ca^{2+}$] dynamics was recorded
648 at 2mM and 11 mM glucose, and first responder cells were identified. Then glucose was lowered
649 to 2mM and [$Ca^{2+}$] activity was monitored to ensure the islet returns to a basal level of activity.
650 The first responder cell(s) were identified, and a sub-cell-sized region of interest to be ablated (5x5
651 μm) was selected either over the first responder cell or over a control cell far from the first
652 responder. Ablation was performed by illuminating the region of interest. [$Ca^{2+}$] dynamics were
653 then imaged during the transition from 2mM to 11mM glucose.
654
655 *Analysis of [$Ca^{2+}$] dynamics:* We defined first responder cells as 10% of the cells imaged within
656 an islet that responded earliest to show elevated [$Ca^{2+}$]. The time of response was defined as time
657 at which intensity of the fluorescence of the [$Ca^{2+}$] indicator (GCaMP6s) reached half the
658 maximum height following islet stimulation by glucose or other secretagogue. We refer to this
659 time as half-height time, or response time throughout the text.
660 The leader and lagger cells were defined during the second-phase [$Ca^{2+}$] response to
661 glucose, once oscillations emerge. These cells were defined based on the phase lag of the slow
662 [$Ca^{2+}$] oscillation in each cell with respect to the phase of the average [$Ca^{2+}$] oscillation across the
663 islet, as previously presented [41]. Islets that lacked second-phase [$Ca^{2+}$] oscillations were
664 excluded from the analysis of the oscillatory phase, and only used for first-phase analysis.

665 For analysis of long term [$Ca^{2+}$] dynamics, only those cells that correspond to cells imaged
666 in the first time point (0 h) were considered. These cells were identified by locating their relative
667 positions with respect to non-β cells which did not express GCaMP6s. Additional cells that appear
668 in the plane of as a result of islets slowly flattening over time were not considered.
669
670 *Distances between the cells:* X and Y coordinates of centers of each ROI outlining a cell were
671 obtained in Fiji software. Then distances between the cells of interest were calculated using these
672 coordinates. In Fig.1 J distance from first responder to first responder indicates average distance
673 between all first responder cells per islet. For example, in the islet shown in Fig.1 I there were
674 several first responding cells (cell #30, #34, …, #48), the distances were measured from cell#48
675 to #30, from #30 to #34, etc. And then the average value was plotted as a dot in Fig.1E (red bar).
676 Similarly, distances between each first responder and other cells of interest were calculated and
677 averaged per islet.
678
679 *Network analysis:* Network connectivity analysis for second-phase [$Ca^{2+}$] response presented in
680 Fig.1 and Fig. S1 was performed by Dr. David Hodson as he reported previously [20] and using
681 the same algorithm. Briefly, [$Ca^{2+}$] time courses were binarized based on intensity deviation from
682 the mean intensity using 20% intensity cutoff. Intensity above this cutoff was assigned a value of
683 1, and below – value of 0. A co-activity matrix with elements $C_{ij}$ for each cell pair in the islet was
684 constructed from the binarized signal.

685 $$C_{ij} = \frac{T_{ij}}{\sqrt{T_i T_j}} \quad (1)$$

686 The $T_i$ and $T_j$ represent time (sec) of activity (when intensity was >20% cutoff) for cells *i* and *j*,
687 and the $T_{ij}$ represents time of co-activity of a cell pair. Then the co-activity matrix was shuffled

688 >9999 times to construct a random co-activity matrix, with elements $C_{ij}^*$, which was used to
689 account for a co-activity being due to chance. The experimental co-activity matrix was then
690 adjusted using threshold constructed of the mean value of $C_{ij}^*$ and a standard deviation from the
691 mean, $\sigma^*$ :

692 $$\mathrm{Thr}_{ij} = \mathrm{C}_{ij}{}^* + 2\sigma^* \quad (2)$$

693 The percent of links was calculated with respect to the maximum number of links per cell
694 in each individual islet. For example, if a most connected cell possessed max=10 links, and other
695 cells had 1, 3, …7 – then % were: 10%, 30%, …70%.

696 Pearson-product-based network analysis presented in Fig.5 was performed as previously
697 reported [21]. [$Ca^{2+}$] time courses were analyzed during the first-phase [$Ca^{2+}$] response, and the
698 analyzed time ranges were chosen to be equal for pre- and post- ablation. The Pearson product for
699 each cell pair in the islet was calculated over each time point, and the time-average values were
700 computed to construct a correlation matrix. An adjacency matrix was calculated by applying a
701 threshold to the correlation matrix. The same threshold of 0.9 was applied to all islets. All cell
702 pairs with a non-zero values in the adjacency matrix were considered to have a functional link.

703

704 *Islet modelling:* The coupled β-cell model was described previously [42] and adapted from the
705 published Cha-Noma single cell model [43, 44]. All code was written in C++ and run on the
706 SUMMIT supercomputer (University of Colorado Boulder).

707 The membrane potential ($V_i$) for each β-cell i is related to the sum of individual ion currents
708 as described by [43]:

709 $$\mathrm{C_m}\frac{\mathrm{dV_i}}{\mathrm{dt}} = \mathrm{I_{Cav}} + \mathrm{I_{TRPM}} + \mathrm{I_{SOC}} + \mathrm{I_{bNSC}} + \mathrm{I_{KDr}} + \mathrm{I_{KCa(SK)}}$$

710 $$+ \mathrm{I_{K_{ATP}}} + \mathrm{I_{NaK}} + \mathrm{I_{NaCa}} + \mathrm{I_{PMCA}} + \mathrm{I_{NaCa}} + \mathrm{I_{Coup}} \quad (3)$$

711 Where the gap junction mediated current $I_{Coup}$ [19] is:

712 $$I_{Coup} = \sum_i g_{Coup}^{ij} (V_i - V_j) \quad (4)$$

713 There are N = 1000 cells in each simulation. Heterogeneity was introduced by randomizing
714 multiple variables according to a Gaussian distribution (Supplemental Table). Heterogeneity in
715 Cx36 gap junctions was modeled as a γ-distribution with parameters k=θ=4 as described
716 previously [22] and scaled to an average $g_{Coup}$ between cells = 120 pS.

717 The flux of glycolysis $J_{glc}$, which is limited by the rate of $k_{glc}$ activity in the β-cell, is
718 described as:

719 $$J_{glc} = k_{glc} \cdot f_{glc} \cdot ([Re_{tot}] - [Re]) \quad (5)$$

720 Where $k_{glc}$ is the maximum rate of glycolysis (equivalent to GK activity), which was simulated as
721 a continuous Gaussian distribution with a mean of 0.000126 $ms^{-1}$ and standard deviation of 25%
722 of the mean. $[Re_{tot}]$ = 10mM, the total amount of pyrimidine nucleotides. The ATP and glucose
723 dependence of glycolysis (GK activity) is:

724 $$f_{glc} = \frac{1}{1+\frac{K_{mATP}}{[ATP]_i}} \cdot \frac{1}{1+\left(\frac{K_G}{[G]}\right)^{hgl}} \quad (6)$$

725 Where [G] is the extracellular concentration of glucose, hgl is the hill coefficient, $K_G$ is the half
726 maximal concentration of glucose, and $K_{mATP}$ is the half maximal concentration of ATP.

727 In simulations where a specific heterogenous parameter is adjusted, the first 100
728 responding cells were determined in a simulation (see below), and these first responder cells were
729 adjusted so that the parameter of choice ($g_{KATP}$, $k_{glc}$, or $g_{Coup}$) was forced to be at the average value
730 (Supplemental Table). The value of the parameter of the other cells in the islet was adjusted so that
731 the average of the parameter value over the islet remained unchanged. A new simulation with these
732 adjusted parameters was run. As a control, a random set of 100 cells are distributed across the islet,

733 and these random cells were selected with the same spatial organization as first responder cells
734 from a simulation that initiated with a different random number seed. These random cells are
735 adjusted in the same way as described above to the average parameter value, while the other cells
736 in the simulation are adjusted so that the average islet value remains unchanged.
737
738 *Islet modelling analysis:* All simulation data analysis was performed using custom MATLAB
739 scripts. First responder cells were determined using the [$Ca^{2+}$] time courses of each cell during the
740 first 20-72 seconds, which covers the first phase [$Ca^{2+}$] response. The response time was calculated
741 as the time to half the maximum [$Ca^{2+}$] level. First responder cells were then determined to be the
742 100 (10%) cells with the earliest response time.
743 In simulations where cells are uncoupled, a given % of cells with the lowest response time
744 are uncoupled from the simulation, but the next 100 cells are analyzed as the first responders of
745 this new simulation. To uncouple cells from the simulated islet, the conductance, $g_{Coup}$, of the cells
746 to be removed is set to 0 pS. Removed cells are excluded from subsequent islet analysis. For
747 control simulations a random % of cells are uncoupled from the islet. These cells are distributed
748 across the islet in the same organization as the first responder cells from a different simulation.
749
750 *Statistical analysis:* All statistical analysis was performed in Prism (GraphPad). For computational
751 results a one-way repeated measures ANOVA with Tukey post-hoc analysis was utilized to test
752 for significant differences between either the WT simulation or a 'Random' control simulation that
753 matched islets before and after parameters are adjusted or cells are uncoupled. For experimental
754 results either one-way ANOVA, or a two-tailed t-test were used (indicated in figure captions) to
755 compare parameters of a specific β-cell subpopulation to the corresponding islet-average

parameters. Data is reported as mean ± s.e.m. (standard error in the mean) unless otherwise indicated. Linear regression analysis was presented as the trend with 95% confidence intervals. The difference of the slope from zero was evaluated with the F test and the p value was reported.

*Sample size estimate*: Power analysis was performed to estimate sample size required for each set of experiment. For example, for experimental set of the relative location of subpopulations (Fig.1D) mean and standard deviation of the distribution of distances from first responder cell to every other first responder in the same islet was chosen as the "expected" group. Power analysis yielded the n=6 per group required to provide the effect size of 20% assuming symmetrical distribution. For the % of functional links (Fig.1) mean and standard deviation of the islet-median % of links distribution was chosen as the "expected" group. Power analysis yielded the n=8 per group required to provide the effect size of 20% assuming symmetrical distribution. In the same fashion mean and standard deviation of the pilot "expected" group were used for power analysis of the rest of the experimental sets (short- and long-term consistency of the response time of the 1$^{st}$ responder, difference in the electrical coupling measured with FRAP, effect of the laser ablation etc). The probability of the type1 error, alpha was chosen as 5%, power was chosen as 80%, and the effect size of 20% was used to estimate sample size through the power analysis.

**Acknowledgments:**

Richard KP Benninger (University of Colorado) is the guarantor of this work and, as such, had full access to all the data in the study and takes responsibility for the integrity of the data and the accuracy of the data analysis. All authors acknowledge that no conflict of interest exists. This work was supported by Juvenile Diabetes Research Foundation (JDRF) Grant 5-CDA-2014-198-A-N; National Institute of Health (NIH) grants R01 DK102950, R01 DK106412 (to RKPB); by JDRF grant 3-PDF-2019-741-A-N (to VK); by NIH grant F31 DK126360 (to JMD). D.J.H. was supported by a Diabetes UK R.D. Lawrence (12/0004431) Fellowship, a Welcome Trust Institutional Support Award, and MRC (MR/N00275X/1 and MR/S025618/1) and Diabetes UK (17/0005681) Project Grants. This project has received funding from the European Research Council (ERC) under the European Union's Horizon 2020 research and innovation program (Starting Grant 715884 to D.J.H.). The funders had no role in the study design, data collection and analysis, decisions to publish, or preparation of the manuscript. We appreciate helpful information on Pearson-based network analysis form Dr. Andraz Stozer, Institute of Physiology, University of Maribor.

**Author Contributions:**

VK conceived of the idea, designed and performed experiments and computer simulations, analyzed data, wrote the manuscript; JMD performed computer simulations, analyzed data, edited text; WES performed animal surgeries, analyzed data; DJH analyzed data, edited the manuscript; RAP performed animal surgeries; AD analyzed data; MSI analyzed data; RKPB conceived of the idea, designed experiments, and wrote the manuscript.

797 **References**


798 [1] D. Salomon and P. Meda, "Heterogeneity and contact-dependent regulation of hormone
799 secretion by individual B cells," (in eng), *Exp Cell Res,* vol. 162, no. 2, pp. 507-20, Feb
800 1986, doi: 10.1016/0014-4827(86)90354-x.
801 [2] E. Bader *et al.*, "Identification of proliferative and mature β-cells in the islets of
802 Langerhans," (in eng), *Nature,* vol. 535, no. 7612, pp. 430-4, 07 2016, doi:
803 10.1038/nature18624.
804 [3] H. Katsuta *et al.*, "Subpopulations of GFP-marked mouse pancreatic β-cells differ in size,
805 granularity, and insulin secretion," (in eng), *Endocrinology,* vol. 153, no. 11, pp. 5180-7,
806 Nov 2012, doi: 10.1210/en.2012-1257.
807 [4] M. Karaca *et al.*, "Exploring functional beta-cell heterogeneity in vivo using PSA-NCAM
808 as a specific marker," (in eng), *PLoS One,* vol. 4, no. 5, p. e5555, 2009, doi:
809 10.1371/journal.pone.0005555.
810 [5] Å. Segerstolpe *et al.*, "Single-Cell Transcriptome Profiling of Human Pancreatic Islets in
811 Health and Type 2 Diabetes," (in eng), *Cell Metab,* vol. 24, no. 4, pp. 593-607, 10 2016,
812 doi: 10.1016/j.cmet.2016.08.020.
813 [6] Y. J. Wang *et al.*, "Multiplexed In Situ Imaging Mass Cytometry Analysis of the Human
814 Endocrine Pancreas and Immune System in Type 1 Diabetes," (in eng), *Cell Metab,* vol.
815 29, no. 3, pp. 769-783.e4, 03 2019, doi: 10.1016/j.cmet.2019.01.003.
816 [7] L. Michon *et al.*, "Involvement of gap junctional communication in secretion," (in eng),
817 *Biochim Biophys Acta,* vol. 1719, no. 1-2, pp. 82-101, Dec 2005, doi:
818 10.1016/j.bbamem.2005.11.003.
819 [8] S. Bavamian *et al.*, "Islet-cell-to-cell communication as basis for normal insulin
820 secretion," (in eng), *Diabetes Obes Metab,* vol. 9 Suppl 2, pp. 118-32, Nov 2007, doi:
821 10.1111/j.1463-1326.2007.00780.x.
822 [9] V. Serre-Beinier *et al.*, "Cx36 preferentially connects beta-cells within pancreatic islets,"
823 (in eng), *Diabetes,* vol. 49, no. 5, pp. 727-34, May 2000, doi: 10.2337/diabetes.49.5.727.
824 [10] R. K. Benninger, M. Zhang, W. S. Head, L. S. Satin, and D. W. Piston, "Gap junction
825 coupling and calcium waves in the pancreatic islet," (in eng), *Biophys J,* vol. 95, no. 11,
826 pp. 5048-61, Dec 2008, doi: 10.1529/biophysj.108.140863.
827 [11] M. A. Ravier *et al.*, "Loss of connexin36 channels alters beta-cell coupling, islet
828 synchronization of glucose-induced Ca2+ and insulin oscillations, and basal insulin
829 release," (in eng), *Diabetes,* vol. 54, no. 6, pp. 1798-807, Jun 2005, doi:
830 10.2337/diabetes.54.6.1798.
831 [12] A. P. Moreno, V. M. Berthoud, G. Pérez-Palacios, and E. M. Pérez-Armendariz,
832 "Biophysical evidence that connexin-36 forms functional gap junction channels between
833 pancreatic mouse beta-cells," (in eng), *Am J Physiol Endocrinol Metab,* vol. 288, no. 5,
834 pp. E948-56, May 2005, doi: 10.1152/ajpendo.00216.2004.
835 [13] S. Speier, A. Gjinovci, A. Charollais, P. Meda, and M. Rupnik, "Cx36-mediated coupling
836 reduces beta-cell heterogeneity, confines the stimulating glucose concentration range,
837 and affects insulin release kinetics," (in eng), *Diabetes,* vol. 56, no. 4, pp. 1078-86, Apr
838 2007, doi: 10.2337/db06-0232.

[14] R. K. Benninger, W. S. Head, M. Zhang, L. S. Satin, and D. W. Piston, "Gap junctions and other mechanisms of cell-cell communication regulate basal insulin secretion in the pancreatic islet," (in eng), *J Physiol,* vol. 589, no. Pt 22, pp. 5453-66, Nov 2011, doi: 10.1113/jphysiol.2011.218909.

[15] J. V. Rocheleau *et al.*, "Critical role of gap junction coupled KATP channel activity for regulated insulin secretion," (in eng), *PLoS Biol,* vol. 4, no. 2, p. e26, Feb 2006, doi: 10.1371/journal.pbio.0040026.

[16] W. S. Head, M. L. Orseth, C. S. Nunemaker, L. S. Satin, D. W. Piston, and R. K. Benninger, "Connexin-36 gap junctions regulate in vivo first- and second-phase insulin secretion dynamics and glucose tolerance in the conscious mouse," (in eng), *Diabetes,* vol. 61, no. 7, pp. 1700-7, Jul 2012, doi: 10.2337/db11-1312.

[17] N. L. Farnsworth, A. Hemmati, M. Pozzoli, and R. K. Benninger, "Fluorescence recovery after photobleaching reveals regulation and distribution of connexin36 gap junction coupling within mouse islets of Langerhans," (in eng), *J Physiol,* vol. 592, no. 20, pp. 4431-46, Oct 2014, doi: 10.1113/jphysiol.2014.276733.

[18] D. G. Pipeleers, "Heterogeneity in pancreatic beta-cell population," (in eng), *Diabetes,* vol. 41, no. 7, pp. 777-81, Jul 1992, doi: 10.2337/diab.41.7.777.

[19] T. H. Hraha, M. J. Westacott, M. Pozzoli, A. M. Notary, P. M. McClatchey, and R. K. Benninger, "Phase transitions in the multi-cellular regulatory behavior of pancreatic islet excitability," *PLoS Comput Biol,* vol. 10, no. 9, p. e1003819, Sep 2014, doi: 10.1371/journal.pcbi.1003819.

[20] N. R. Johnston *et al.*, "Beta Cell Hubs Dictate Pancreatic Islet Responses to Glucose," (in eng), *Cell Metab,* vol. 24, no. 3, pp. 389-401, 09 2016, doi: 10.1016/j.cmet.2016.06.020.

[21] A. Stožer *et al.*, "Functional connectivity in islets of Langerhans from mouse pancreas tissue slices," (in eng), *PLoS Comput Biol,* vol. 9, no. 2, p. e1002923, 2013, doi: 10.1371/journal.pcbi.1002923.

[22] M. J. Westacott, N. W. F. Ludin, and R. K. P. Benninger, "Spatially Organized beta-Cell Subpopulations Control Electrical Dynamics across Islets of Langerhans," *Biophys J,* vol. 113, no. 5, pp. 1093-1108, Sep 5 2017, doi: 10.1016/j.bpj.2017.07.021.

[23] R. K. Benninger *et al.*, "Intrinsic islet heterogeneity and gap junction coupling determine spatiotemporal $Ca^{2+}$ wave dynamics," (in eng), *Biophys J,* vol. 107, no. 11, pp. 2723-33, Dec 2014, doi: 10.1016/j.bpj.2014.10.048.

[24] V. Salem *et al.*, "Leader β-cells coordinate Ca," (in eng), *Nat Metab,* vol. 1, no. 6, pp. 615-629, Jun 2019, doi: 10.1038/s42255-019-0075-2.

[25] D. L. Curry, L. L. Bennett, and G. M. Grodsky, "Dynamics of insulin secretion by the perfused rat pancreas," (in eng), *Endocrinology,* vol. 83, no. 3, pp. 572-84, Sep 1968, doi: 10.1210/endo-83-3-572.

[26] D. Porte and A. A. Pupo, "Insulin responses to glucose: evidence for a two pool system in man," (in eng), *J Clin Invest,* vol. 48, no. 12, pp. 2309-19, Dec 1969, doi: 10.1172/JCI106197.

[27] J. C. Henquin, "Relative importance of extracellular and intracellular calcium for the two phases of glucose-stimulated insulin release: studies with theophylline," (in eng), *Endocrinology,* vol. 102, no. 3, pp. 723-30, Mar 1978, doi: 10.1210/endo-102-3-723.

[28] C. S. Nunemaker, D. H. Wasserman, O. P. McGuinness, I. R. Sweet, J. C. Teague, and L. S. Satin, "Insulin secretion in the conscious mouse is biphasic and pulsatile," (in eng), *Am J Physiol Endocrinol Metab,* vol. 290, no. 3, pp. E523-9, Mar 2006, doi: 10.1152/ajpendo.00392.2005.

[29] C. S. Nunemaker *et al.*, "Individual mice can be distinguished by the period of their islet calcium oscillations: is there an intrinsic islet period that is imprinted in vivo?," (in eng), *Diabetes,* vol. 54, no. 12, pp. 3517-22, Dec 2005, doi: 10.2337/diabetes.54.12.3517.

[30] C. S. Nunemaker *et al.*, "Glucose metabolism, islet architecture, and genetic homogeneity in imprinting of [Ca2+](i) and insulin rhythms in mouse islets," (in eng), *PLoS One,* vol. 4, no. 12, p. e8428, Dec 2009, doi: 10.1371/journal.pone.0008428.

[31] M. Zhang, P. Goforth, R. Bertram, A. Sherman, and L. Satin, "The Ca2+ dynamics of isolated mouse beta-cells and islets: implications for mathematical models," (in eng), *Biophys J,* vol. 84, no. 5, pp. 2852-70, May 2003, doi: 10.1016/S0006-3495(03)70014-9.

[32] J. Zmazek *et al.*, "Assessing Different Temporal Scales of Calcium Dynamics in Networks of Beta Cell Populations," (in eng), *Front Physiol,* vol. 12, p. 612233, 2021, doi: 10.3389/fphys.2021.612233.

[33] A. Vogel and V. Venugopalan, "Mechanisms of pulsed laser ablation of biological tissues," (in eng), *Chem Rev,* vol. 103, no. 2, pp. 577-644, Feb 2003, doi: 10.1021/cr010379n.

[34] J. M. Dwulet *et al.*, "How Heterogeneity in Glucokinase and Gap-Junction Coupling Determines the Islet [Ca," (in eng), *Biophys J,* vol. 117, no. 11, pp. 2188-2203, 12 2019, doi: 10.1016/j.bpj.2019.10.037.

[35] R. K. P. Benninger and D. J. Hodson, "New Understanding of β-Cell Heterogeneity and In Situ Islet Function," (in eng), *Diabetes,* vol. 67, no. 4, pp. 537-547, 04 2018, doi: 10.2337/dbi17-0040.

[36] H. Modi, "Ins2 gene bursting activity defines a mature β-cell state," BioRxiv, 2019.

[37] V. Serre-Beinier *et al.*, "Cx36 makes channels coupling human pancreatic beta-cells, and correlates with insulin expression," (in eng), *Hum Mol Genet,* vol. 18, no. 3, pp. 428-39, Feb 2009, doi: 10.1093/hmg/ddn370.

[38] J. M. Dwulet, J. K. Briggs, and R. K. P. Benninger, "Small subpopulations of β-cells do not drive islet oscillatory [Ca 2+ ] dynamics via gap junction communication," vol. https://doi.org/10.1101/2020.10.28.358457, ed. BioRXiv, 2020.

[39] C. Dorrell *et al.*, "Human islets contain four distinct subtypes of β cells," (in eng), *Nat Commun,* vol. 7, p. 11756, 07 2016, doi: 10.1038/ncomms11756.

[40] K. Shekiro , T. H. Hraha , A. B. Bernard , R. K. Benninger , and K. S. Anseth "Engineering Functional Pseudo-Islets of Defined Sizes from Primary Murine Cells Using PEG Microwell Devices," ed, 2020.

[41] M. J. Westacott, N. W. F. Ludin, and R. K. P. Benninger, "Spatially Organized β-Cell Subpopulations Control Electrical Dynamics across Islets of Langerhans," (in eng), *Biophys J,* vol. 113, no. 5, pp. 1093-1108, Sep 2017, doi: 10.1016/j.bpj.2017.07.021.

[42] J. M. Dwulet *et al.*, "How Heterogeneity in Glucokinase and Gap-Junction Coupling Determines the Islet [Ca(2+)] Response," *Biophys J,* vol. 117, no. 11, pp. 2188-2203, Dec 3 2019, doi: 10.1016/j.bpj.2019.10.037.

[43] C. Y. Cha *et al.*, "Ionic mechanisms and Ca2+ dynamics underlying the glucose response of pancreatic beta cells: a simulation study," (in English), *J Gen Physiol,* vol. 138, no. 1, pp. 21-37, Jul 2011, doi: DOI 10.1085/jgp.201110611.

[44] C. Y. Cha, E. Santos, A. Amano, T. Shimayoshi, and A. Noma, "Time-dependent changes in membrane excitability during glucose-induced bursting activity in pancreatic beta cells," (in eng), *J Gen Physiol,* vol. 138, no. 1, pp. 39-47, Jul 2011, doi: 10.1085/jgp.201110612.

## Supplemental Figures

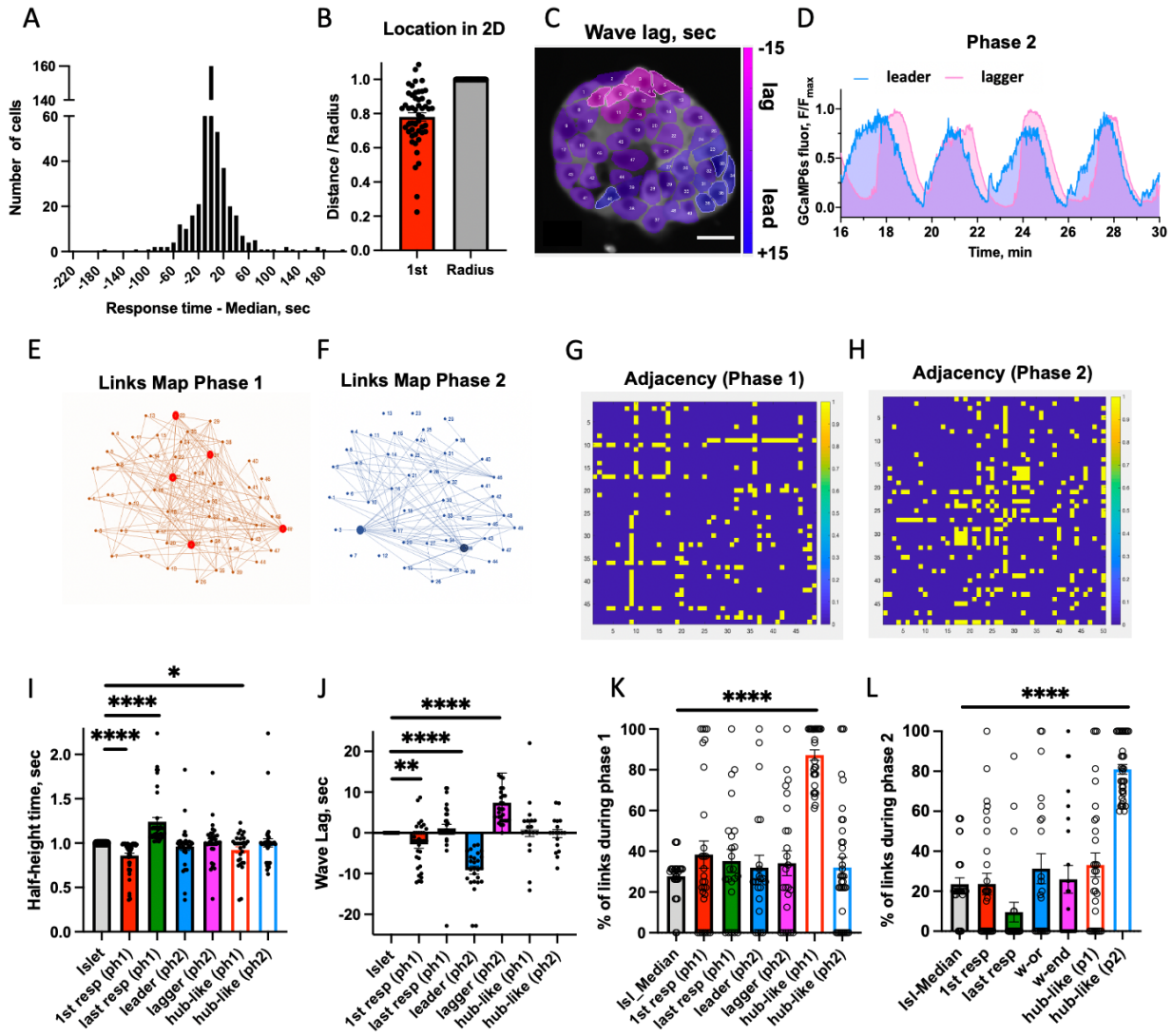


**Figure S1**. A) Cumulative response time (Tresp) distribution for 19 islets. B) Location of 1st responder cells in the 2D islet plane, normalized by islet radius. C) Representative false-color map of calcium phase lag. D) Example of calcium leader and "lagger" cell time traces. E) and F) link maps obtained using network analysis for first- and second-phase calcium response, correspondingly. G) and H) Adjacency matrices for for first- and second-phase calcium response, correspondingly. I) [$Ca^{2+}$] response time to glucose elevation for different beta-cell states (n=8-10 islets, m=30-45 cells). J) Phase lag of the $Ca^{2+}$ wave with respect to the islet-average wave for different beta-cell states (n=8-12 islets, m=18-34 cells). K), L) Coordination (network) analysis for n=8 islets performed for first- and second-phase calcium dynamics, correspondingly. Functional network analysis was performed via binarization and co-activity matrix analysis, as described before [20]. Statistical tests: I, J: one-sample t-test, K, L: ordinary one-way ANOVA where **** represents $p<0.0001$, *** $p<0.0002$, ** $p<0.0021$, * $p<0.0332$ indicated for comparison of the groups.

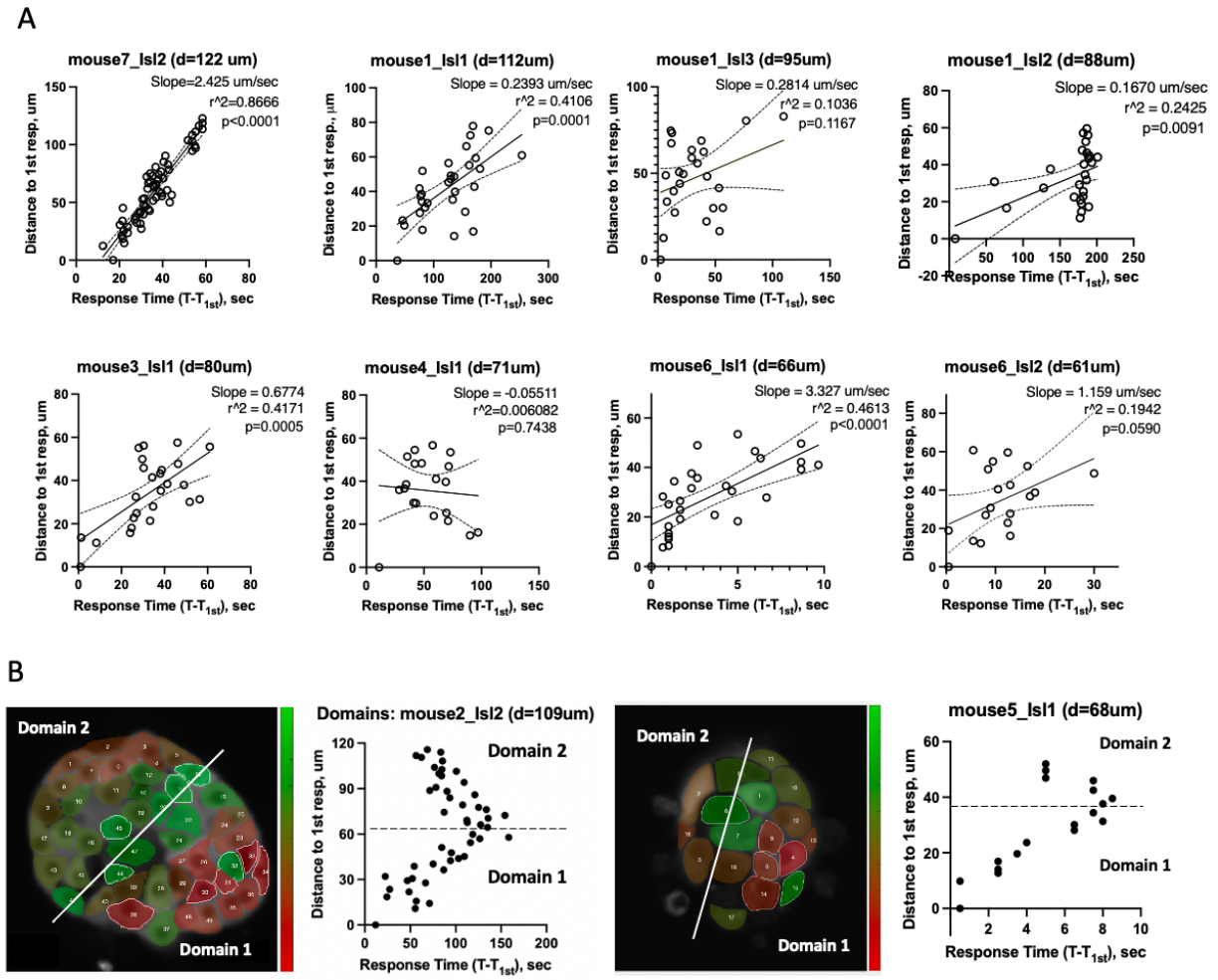


**Figure S2**. A) Correlation between the absolute response time of each beta-cell in an islet and their proximity to the first responder beta-cell, for 8 islets. Solid line indicates regression, dashed line indicates 95% CI. E) Examples of islets in which there are 2 domains with local first responder clusters per each domain, as well as distance of each cell in the islet plane to 1st responders (located in Domain1) vs time of response to glucose.

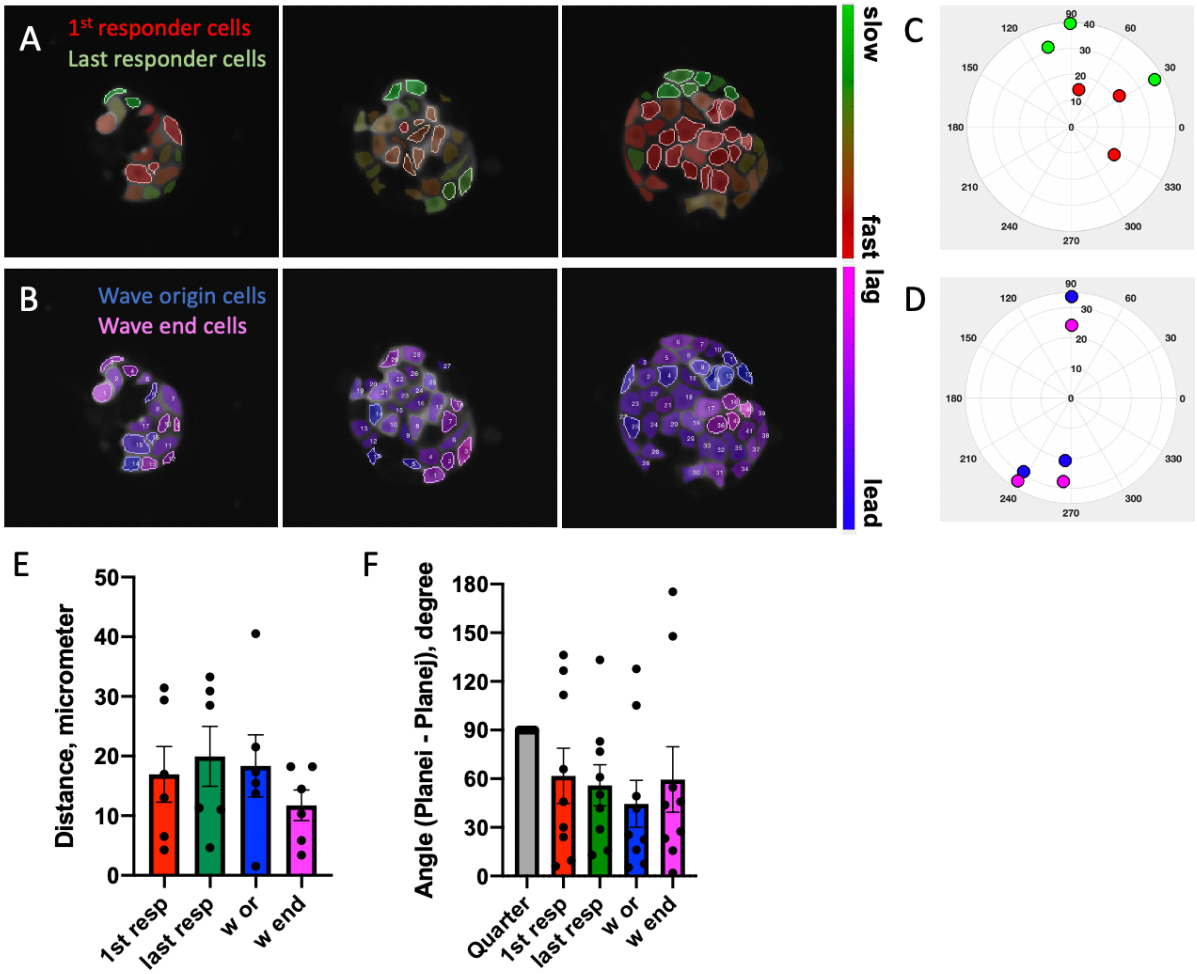


**Figure S3**. A) Pseudo-color map representing time of response to glucose during the first-phase [$Ca^{2+}$] response in three adjacent planes in the islet separated by 10 µm. First and last responder cells are highlighted with the white borders. B) Pseudo-color map representing wave propagation in the same islet planes during the second-phase [$Ca^{2+}$] response. Wave origin and wave end cells are highlighted with the white borders. C), D) Plane-average positions of each beta cell subpopulation for three planes. E) Distances between the plane-average positions of each subpopulation (position in plane (i) – position in plane (j)). Average distances are ~20 µm, indicating that location of all four subpopulations of interest is conserved in 3D. F) Polar angle between the plane-average positions of the subpopulations (angle in plane (i) – angle in plane (j)). Average angles are below 90 degrees, indicating spatial conservation of the location of all four subpopulations of interest in 3D. For (E,F) n=4 islets were studied.

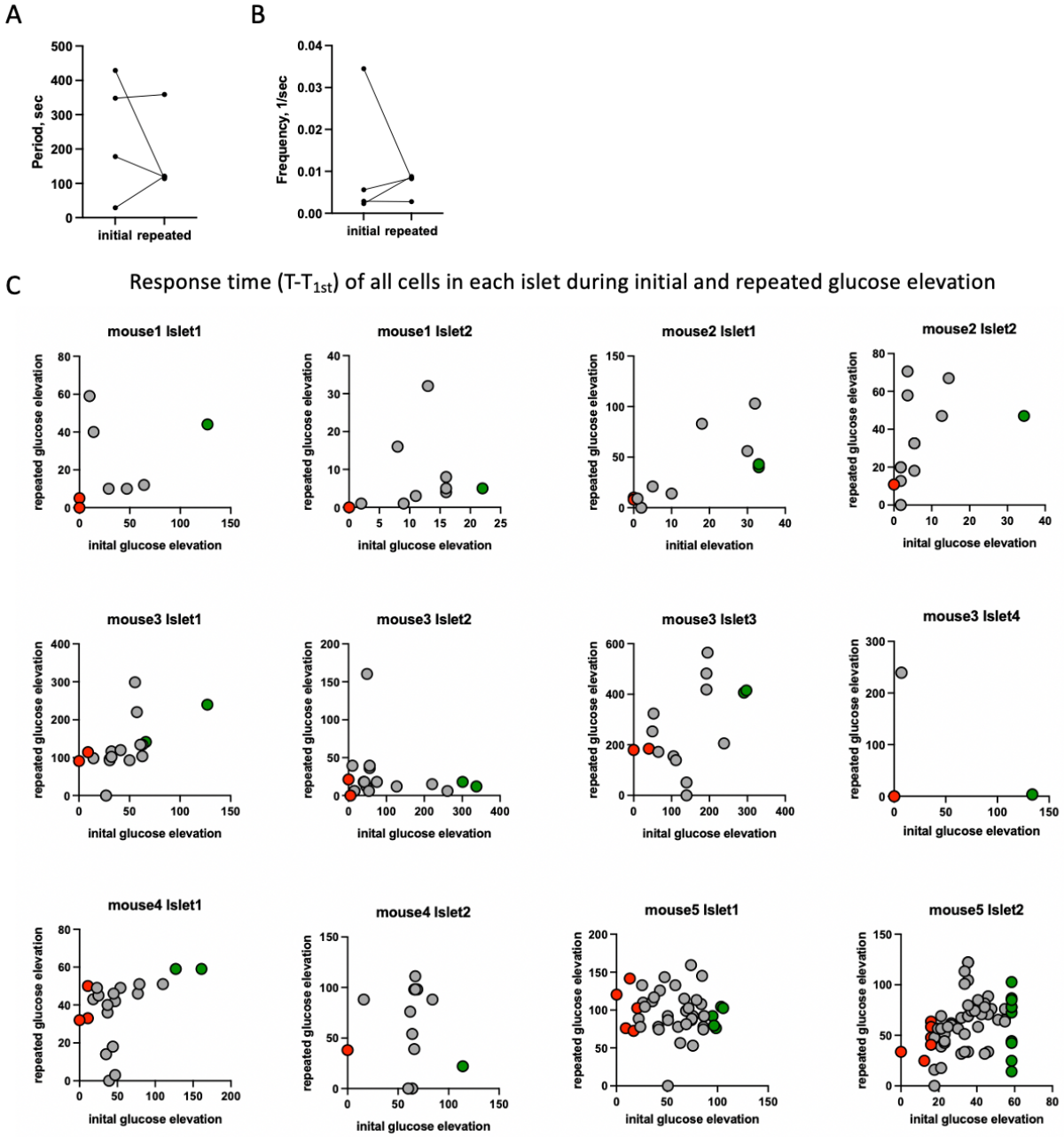


**Figure S4**. A) Quantification of the $Ca^{2+}$ oscillation period and B) frequency during initial and repeated glucose elevation (n=4 islets). No significant difference was found in one sample t-test with initial-repeated period (frequency) difference compared to 0. C) Response time of all cells in the optical section of the islet during initial vs during repeated glucose elevation. Red dots represent first responder, and green – last responder cells identified during the initial glucose elevation.

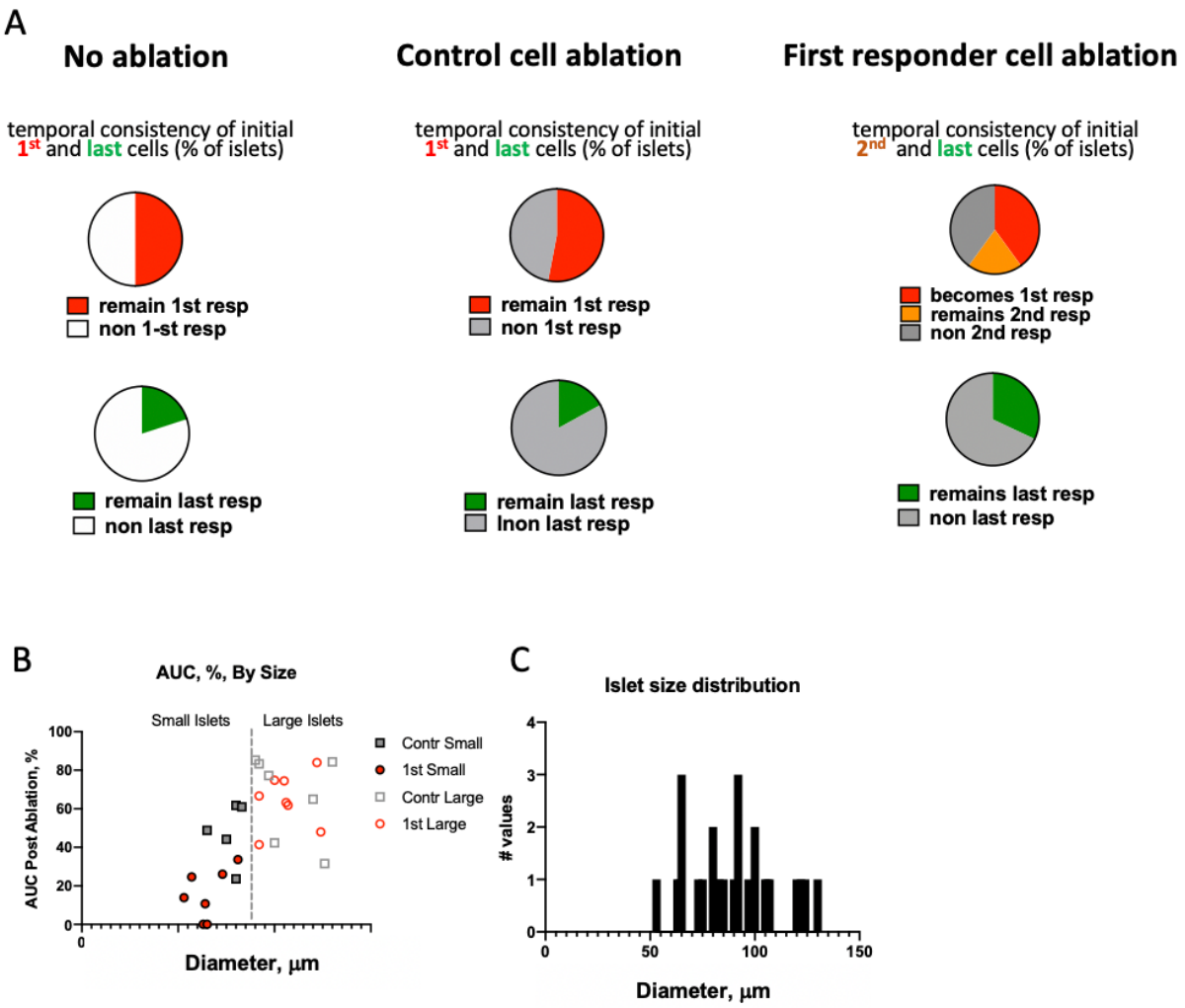


**Figure S5**. A) Left Pie chart: Percent of islets in which initial first and last responders remain in their role during repeated glucose elevation. Middle Pie chart: same as Left but following control cell ablation. Right Pie charts: same as middle but following first responder cell ablation. B) Islet size dependence of the $[Ca^{2+}]$ influx into the islet (area under the curve of the $[Ca^{2+}]$ time-course) for random and first responder ablation cases. D) Size distribution of the islets studied in the ablation experiments.

| Parameter | Description of parameter | Distribution | Mean ± Std Dev | units |
|---|---|---|---|---|
| $g_{KATP}$ | Max conductance of $K_{ATP}$ channel current | Normal | 2.31 ± 0.57 | pA $mV^{-1}$ |
| $k_{glc}$ | Rate constant of glycolysis | Normal | 0.000126 ± 0.0000315 | $ms^{-1}$ |
| $g_{Coup}$ | Coupling conductance | Gamma, k=θ=4 | 120 ± 30 | ps |
| $g_{KTO}$ | Conductance of $I_{KCa(BK)}$ (voltage and $Ca^{2+}$) dependent transient outward $K^+$ current | Normal | 2.13 ± 0.213 | pA $mV^{-1}$ |
| $P_{SERCA}$ | Maximum rate of pumping $Ca^{2+}$ into ER | Normal | 0.096 ± 0.0096 | amole $ms^{-1}$ |
| $P_{NaCa}$ | Maximum amplitude of $I_{NaCa}$, $Na^+/Ca^{2+}$ exchanger | Normal | 204 ± 20 | pA |
| $P_{rel}$ | Converting factor for $Ca^{2+}$ release from ER | Normal | 0.46 ± 0.46 | fl $ms^{-1}$ |
| $P_{op}$ | Maximum rate of ATP production from oxphos | Normal | 0.0005 ± 0.00005 | $ms^{-1}$ |
| $[ATP_{tot}]$ | Total amount of ATP species | Normal | 4 ± 0.4 | mM |

**Supplemental Table**. Values of heterogeneous parameters used in the islet simulations.

**List of Source Data Files:**

Figure 1 – Source Data (values used for all graphs in Figure 1)

Figure 2 – Source Data (values used for all graphs in Figure 2)

Figure 3 – Source Data (values used for all graphs in Figure 3)

Figure 4 – Source Data (values used for all graphs in Figure 4)

Figure 5 – Source Data (values used for all graphs in Figure 5)

Figure 6 – Source Data (values used for all graphs in Figure 6)

Statistical analysis (Summary of statistical analysis for Figures 1-6)

KATP_MovetoAvg_seed1 (model code for Figure 6 I, J)

Coup_MovetoAvg_seed1 (model code for Figure 6 I, J)

Uncouple_FirstResp_Seed1_perc20 (model code for Figure 6 L)